

A Realistic Determination of the Error on the Primordial Helium Abundance: Steps Toward Non-Parametric Nebular Helium Abundances

Keith A. Olive

*William I. Fine Theoretical Physics Institute,
University of Minnesota, Minneapolis, MN 55455, USA*

olive@umn.edu

Evan D. Skillman

Astronomy Department, University of Minnesota, Minneapolis, MN 55455

skillman@astro.umn.edu

ABSTRACT

Using the WMAP determination of the baryon density, the standard model of big bang nucleosynthesis yields relatively precise predictions of the primordial light element abundances. Currently there are two significantly different observational determinations of the primordial helium abundance, and, if only statistical errors in ^4He abundance determinations are considered, the discrepancies between the observational determinations and the value favored by the WMAP results are significant. Here we examine in detail some likely sources of systematic uncertainties which may resolve the differences between the two determinations. We conclude that the observational determination of the primordial helium abundance is completely limited by systematic errors and that these systematic errors have not been fully accounted for in any published observational determination of the primordial helium abundance. In principle, the observed metal-poor HII region spectra should be analyzed in a non-parametric way, such that the HII region physical conditions and the helium abundance are derived solely from the relative flux ratios of the helium and hydrogen emission lines. In practice, there are very few HII region spectra with the quality that allow this, so that most analyses depend on assumed ranges or relationships between physical parameters, resulting in parametric solutions with underestimated error bars. A representative result of our analysis yields $Y_p = 0.249 \pm 0.009$. However, given that most of the spectra analyzed to date do not significantly constrain the primordial helium abundance, we argue in favor a range of allowed values of $0.232 \leq Y_p \leq 0.258$. This easily allows for concordance between measurements of the baryon-to-photon ratio (η) from WMAP, deuterium abundances, and helium abundance (although the discrepancy with lithium remains).

Subject headings: HII Regions: abundances — galaxies: abundances — cosmology: early universe

1. Introduction

The standard model for cosmology can be described by a small number of parameters, and relatively accurate determinations of many of those parameters are now available. Recently, cosmic microwave background experiments, most notably WMAP, have determined the primordial spectrum of density fluctuations down to small angular scales with excellent agreement with galaxy and cluster surveys (Bennett *et al.* 2003; Spergel *et al.* 2003). The overall curvature of the Universe is determined to be $\Omega = \rho/\rho_c = 1$ within a few percent, where $\rho_c = 3H^2/8\pi G_N$. The evolution of the Universe (past, present, and future) also depends on the composition of matter in the Universe: radiation, baryons, cold dark matter, a cosmological constant or dark energy. Agreement between CMB measurements, Supernovae Type I data (Riess *et al.* 1999; Perlmutter *et al.* 1999; Tonry *et al.* 2003), and clustering data (Percival 2002; Tegmark *et al.* 2003) are concordant with $\Omega_\Lambda : \Omega_m$ approximately 2:1. Here, we are interested in the redundancies in the determination of the baryon density, Ω_B , using both the CMB and big bang nucleosynthesis (BBN) (Walker *et al.* 1991; Sarkar 1996; Olive, Steigman, & Walker 2000; Fields & Sarkar 2002).

The baryon density (or the baryon-to-photon ratio, $\eta \equiv \eta_{10}/10^{10}$) is the sole parameter in the standard model of BBN. Prior to the recent high accuracy measurements of the microwave background power spectrum, the best available method for determining the baryon density of the Universe was the concordance of the BBN predictions and the observations of the light element abundances of D, ^3He , ^4He , and ^7Li . A high-confidence upper limit to the baryon density has long been available (Reeves *et al.* 1976) from observations of local D/H abundance determinations (giving roughly $\eta_{10} < 9.0$), but a reliable lower bound to η , much less a precise value, has been problematic. Observations of each of the light elements D, ^4He , and ^7Li can be used individually to determine the value of η . Confidence in any such determination, however, relies on the concordance of the three light isotopes. Likelihood analyses (Fields & Olive 1996; Fields *et al.* 1996; Hata *et al.* 1997; Fiorentini *et al.* 1998; Esposito *et al.* 2000; Cyburt, Fields, & Olive 2001; Burles, Nollett, & Turner 2001) using the combined ^4He , ^7Li and D/H observations enable one to determine a 95 % CL range of $5.1 < \eta_{10} < 6.7$ with a most likely value of $\eta_{10} = 5.7$ corresponding to $\Omega_B h^2 = 0.021$. However, one concern regarding the likelihood method is the relatively poor agreement between ^4He and ^7Li on the one hand and D on the other. The former two taken alone indicate that the most likely value for η_{10} is 2.4, while D/H alone implies a best value of 6.1. This discrepancy may point to new

physics, but could well be due to underestimated systematic errors in the observations. Recently, more weight has been given to the D/H determinations because of their excellent agreement with the CMB experiments.

In the past few years, balloon and ground-based observations have made the first observations at multipoles $\ell \gtrsim 200$, where the sensitivity to η lies, and determinations of η at the 20 % level became possible (Netterfield *et al.* 2002; Abroe *et al.* 2002; Pryke *et al.* 2002; Sievers *et al.* 2002; Rubiño-Martin *et al.* 2003; Goldstein *et al.* 2002; Benoit *et al.* 2002). With WMAP (Bennett *et al.* 2003; Spergel *et al.* 2003), the CMB-based inference of the baryon-to-photon ratio is $\Omega_B h^2 = 0.0224 \pm 0.0009$, or $\eta_{10, \text{CMB}} = 6.14 \pm 0.25$ – a precision of 4%. This estimate is the best-fit WMAP value, which is sensitive mostly to WMAP alone (primarily the first and second acoustic peaks) but does include CBI (Sievers *et al.* 2002) and ACBAR (Goldstein *et al.* 2002) data on smaller angular scales. Note, however, that there is a small and marginally significant difference between the values of η derived by using only the WMAP data or using the WMAP data in combination with other observations (Spergel *et al.* 2003) as shown here in Figure 1.

One can use $\eta_{10, \text{CMB}}$ as an input to BBN calculations and predict the primordial abundances of the light elements. This yields relatively precise abundances (Cyburt *et al.* 2003):

$$\begin{aligned}
 (\text{D}/\text{H})_p &= 2.75_{-0.19}^{+0.24} \times 10^{-5} \\
 {}^3\text{He}/\text{H} &= 9.28_{-0.54}^{+0.55} \times 10^{-6} \\
 Y_p &= 0.2484_{-0.0005}^{+0.0004} \\
 {}^7\text{Li}/\text{H} &= 3.82_{-0.60}^{+0.73} \times 10^{-10}
 \end{aligned}
 \tag{1}$$

Because there are no measurements of ${}^3\text{He}$ at very low metallicity (i.e., significantly below solar) at this time, a higher burden is placed on the remaining three elements. The D/H prediction is in excellent agreement with the average of the five best determined quasar absorption system abundances (Burles & Tytler 1998a,b; O’Meara *et al.* 2001; Pettini & Bowen 2001; Kirkman *et al.* 2003) which give $\text{D}/\text{H} = (2.78 \pm 0.29) \times 10^{-5}$ (see Figure 1). In contrast, the ${}^7\text{Li}$ prediction is rather high. The results of Ryan, Norris, & Beers (1999), give ${}^7\text{Li}/\text{H} = 1.23_{-0.16}^{+0.34} \times 10^{-10}$ which is a factor of 3 below the WMAP value, and almost a factor of 2 below even when systematics are stretched to maximize the ${}^7\text{Li}$ abundance (Ryan *et al.* 2000). Even a recent study (Bonifacio *et al.* 2002) with temperatures based on $\text{H}\alpha$ lines (considered to give systematically high temperatures) yields ${}^7\text{Li}/\text{H} = (2.19 \pm 0.28) \times 10^{-10}$. Recent attempts (Coc *et al.* 2004, Cyburt, Fields, & Olive 2004) to ascribe this discrepancy to systematic uncertainties in the relevant nuclear rates for ${}^7\text{Li}$

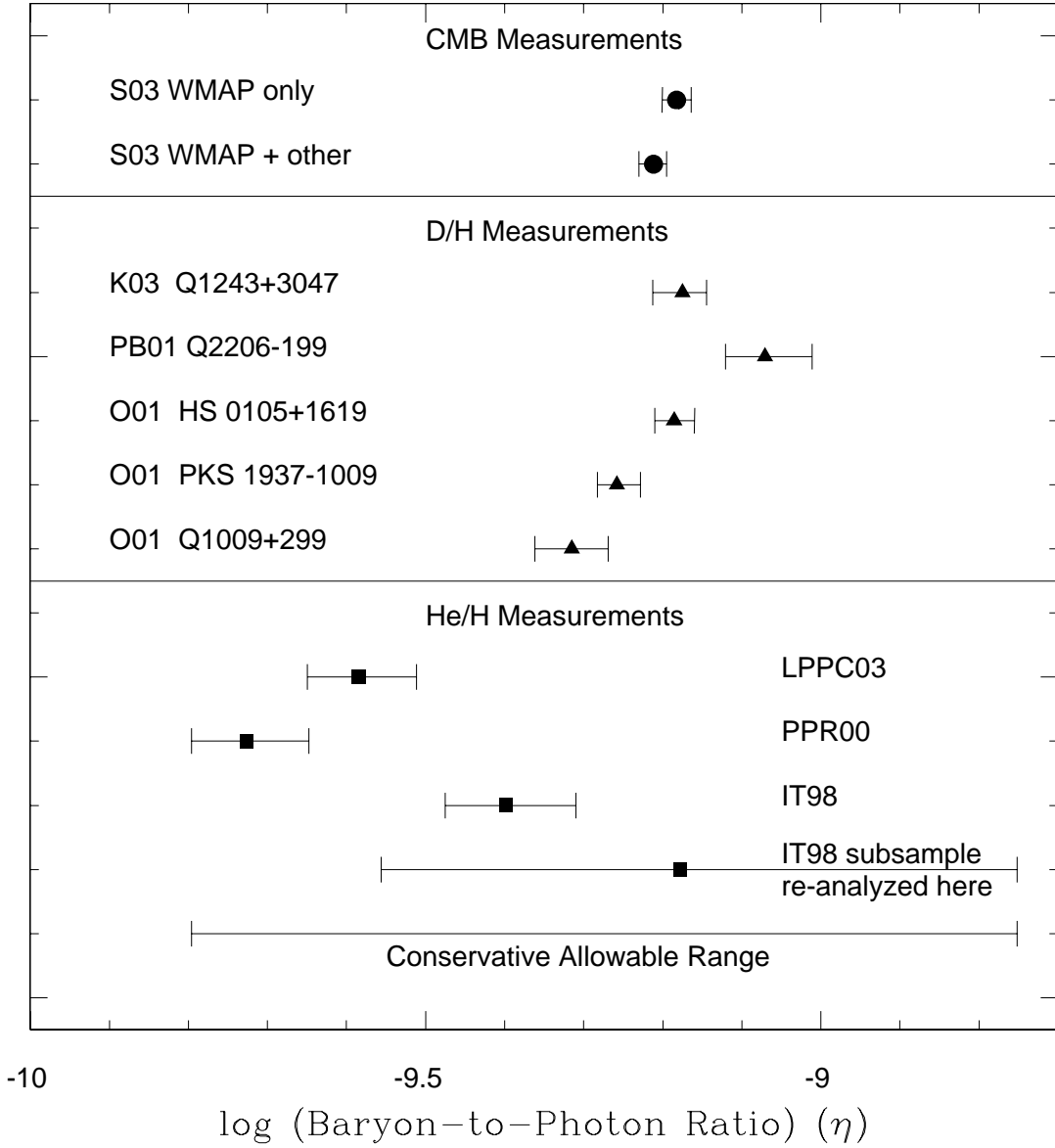


Fig. 1.— The various observational limits on the value of the baryon-to-photon ratio (η) individually plotted. The value derived from He/H measurements labeled IT98 represents the results from 45 independent measurements while the value labeled IT98 re-analyzed represents the value determined from a reanalysis of the seven highest quality measurements from that sample. The recommended conservative range extends the range from the IT98 re-analysis to the lowest values determined by Peimbert and collaborators.

show that this is unlikely. Of course, some of the discrepancy may be due to Li depletion in the stellar atmosphere (Vauclair & Charbonnel 1998, Pinsonneault *et al.* 1999, 2002). Finally, the predicted ${}^4\text{He}$ abundance is also rather high when compared to the large body of data on ${}^4\text{He}$ in extragalactic HII regions.

Given the concordance of the WMAP determinations with the average of the D/H determinations, is the value of η secure, and thus, should the topic be considered closed? There are a number of reasons that we feel that it is important to resolve the differences indicated in Figure 1. First, it is important to remember that individual cosmological parameters cannot be derived independently from microwave background measurements; the microwave background measurements constrain combinations of cosmological parameters. Thus, independent constraints on individual parameters (or, in this case, the combination of just two parameters - $\Omega_B h^2$) continue to be very important. Second, the concordance of the primordial abundances of the light elements has long been regarded as a triumph of modern cosmology, and thus, regaining concordance remains an important goal. Finally, there are some aspects of the η determinations that bear further inspection. One example is the previously mentioned small difference between the value derived from WMAP alone and that derived from combining in other observations. Another example, also shown in Figure 1, is the fact that the error bars on the individual D/H η determinations, in many cases, are not overlapping, and averaging the five best determined absorption systems may not be the correct way to treat the data. The dispersion in the D/H data may be a result of chemical evolution or underlying systematic uncertainties in the observations (Fields *et al.* 2001). Thus, we feel that the problem of the concordance of the various determinations of η is an important one, and here we will concentrate on the determination of the value of the primordial helium abundance.

Unlike the other light element abundances, in order to be a useful cosmological constraint, ${}^4\text{He}$ needs to be measured with a precision at the few percent level. Thus, the determination of the ${}^4\text{He}$ abundance has become limited by systematic uncertainties. To date, the most useful ${}^4\text{He}$ abundance determinations are made by observing helium emission lines in HII regions of metal-poor dwarf galaxies.

Izotov & Thuan (1998, hereafter IT98) assembled a sample of 45 low metallicity HII regions, observed and analyzed in a uniform manner, and derived a value of $Y_p = 0.244 \pm 0.002$ and 0.245 ± 0.001 (with regressions against O/H and N/H respectively)¹. This value is significantly higher than the value of $Y_p = 0.228 \pm 0.005$ derived by Pagel *et al.* (1992, hereafter PSTE) using nearly

¹This data set was recently extended to include 82 HII regions obtaining similar results (Izotov & Thuan 2004).

identical analysis techniques. Peimbert, Peimbert, & Ruiz (2000, hereafter PPR00) have derived a very accurate helium abundance for the HII region NGC 346 in the Small Magellanic Cloud, and from this they infer a value of $Y_p = 0.2345 \pm 0.0026$. PPR00 take a fundamentally different approach to determining the electron temperature (compared to PSTE and IT98). Specifically, they use the He I emission lines to solve for the electron temperature (resulting in a lower temperature than indicated by the [O III] lines, in line with predictions from photoionization models) and include the effects of estimating the amplitude of temperature fluctuations. Thus, these two different results depend not only on different observations, but also on differences in the analyses of the observations. Recently, Luridiana et al. (2003, hereafter LPPC) have analyzed spectra of five metal poor HII regions and, after considering the effects of additional physical processes (e.g., collisional excitation of the Balmer lines), have produced a higher (compared to PPR00) determination of $Y_p = 0.239 \pm 0.002$. As shown in Figure 1, this higher value is still significantly lower than the value derived by IT98 or from the WMAP observations. We are left with the conundrum in that the studies that appear to have the higher quality observations and the more complete physical analysis (PPR00 and LPPC) arrive at a answer which is further from concordance with WMAP results (relative to IT98).

One approach to the problem would be to assume that the CMB measurements are providing us with the correct value of Ω_B , and then BBN allows us to calculate the corresponding value of Y_p (Cyburt, Fields, & Olive 2002, 2003). Assuming that this is correct, we may be better able to understand the systematic effects in the determination of Y_p from nebular spectroscopy.

In an earlier paper, (Olive & Skillman 2001, hereafter OS) we critically examined the “self-consistent” approach of determining the ^4He abundance used by IT98, and concluded that uncertainties were systematically underestimated, especially with regard to the treatment of underlying stellar absorption (see also Skillman, Terlevich, & Terlevich 1998). This effect alone could be sufficient to explain the discrepancy between the IT98 result and the WMAP result, but it is unlikely to resolve the difference between the IT98 and PPR00 studies. Additionally, Benjamin, Skillman, & Smits (2002) have presented new calculations of HeI radiative transfer effects and have shown that some of the fitting formulae introduced by IT98 had significant errors.

In this paper, we will attempt to better quantify the true uncertainties in the individual helium determinations in extragalactic HII regions and hopefully produce a more secure estimate of Y_p . We present an update of our minimization procedure, adding in the ability to solve self-consistently for the electron temperature. The new calculations of radiative transfer effects are also incorporated

into this new code. The goal of this paper is to explore different analysis methodologies and to promote particular analysis techniques in order to carefully assess the true systematic uncertainty in ^4He abundance determinations.

2. A New Minimization Code

In our previous work (OS), in order to make calculations directly comparable to those of IT98, we used the H I emissivities calculated by Hummer & Storey (1987), the He I emissivities calculated by Smits (1996), the collisional rates of Sawey & Berrington (1993), the resulting collisional corrections calculated by Kingdon & Ferland (1995), and the He I radiative transfer model of IT98 based on Robbins (1968). Here, these are replaced and combined by new calculations from Benjamin, Skillman, & Smits (1999; 2002). While the emissivity and collisional corrections presented by Benjamin, Skillman, & Smits (1999) did not result in large changes relative to previous values, the new radiative transfer model presented in Benjamin, Skillman, & Smits (2002) is substantially different from that of IT98. As detailed in our previous paper, we also allow for the possibility of underlying stellar absorption. The details used in computing the helium abundance are given in the Appendix.

The self consistent method we employ makes use of six He emission lines: $\lambda 3389$, $\lambda 4026$, $\lambda 4471$, $\lambda 5876$, $\lambda 6678$, $\lambda 7026$. The ratio of each He I emission line intensity to $\text{H}\beta$ is compared to the theoretical ratio and corrected for the effects of collisional excitation, fluorescence, and underlying He I absorption. From these line ratios, we need to determine three physical parameters, the density, n , the optical depth, τ , and the equivalent width for underlying helium absorption, a_{HeI} . In OS, we had assumed an input temperature (typically derived from [O III] emission lines). As pointed out in PPR00, the temperature dependences of the He I emissivities are exponential and can be both positive and negative, so that the relative He I lines can provide a strong temperature diagnostic (which will be more appropriate to the He^+ zone). Thus, our new procedure allows us to solve for the temperature as we do for the other physical parameters.

As described in detail in OS, we use the derived He abundances $y^+(\lambda)$ to compute the average helium abundance, \bar{y} ,

$$\bar{y} = \sum_{\lambda} \frac{y^+(\lambda)}{\sigma(\lambda)^2} / \sum_{\lambda} \frac{1}{\sigma(\lambda)^2} \quad (2)$$

This is a weighted average, where the uncertainty $\sigma(\lambda)$ is found by propagating the uncertainties in the observational quantities stemming from the observed line fluxes (which already contains the

uncertainty due to $C(H\beta)$, and the equivalent widths.

From \bar{y} , we can define a χ^2 as the deviation of the individual He abundances $y^+(\lambda)$ from the average,

$$\chi^2 = \sum_{\lambda} \frac{(y^+(\lambda) - \bar{y})^2}{\sigma(\lambda)^2} \quad (3)$$

We then minimize χ^2 , to determine n, a_{HeI} , and τ and the temperature, T . Uncertainties in the output parameters are determined by varying the outputs until $\Delta\chi^2 = 1$.

The real challenge for the new code is determining the correct combination of temperature and density. While it is true, in principle, that the He I lines can provide a strong temperature diagnostic, in practice, this requires very precise emission line fluxes to pin down the temperature to a narrow range. The difficulty comes from the fact that the three strong lines which form the backbone of the solution ($\lambda 5876$, $\lambda 4471$, and $\lambda 6678$) all have the same sense of temperature and density dependence, i.e.,

$$F_{HeI} = AT^{B-Cn_e} \quad (4)$$

where A, B, and C are positive constants. Because the three main lines (and $\lambda 4026$) all behave in similar ways, there is a natural tendency towards solutions combining either high temperatures and low densities or low temperatures and high densities. Thus, if temperatures are systematically overestimated (as is probably true if one assumes the temperature derived from the [O III] lines), then the solutions are forced systematically to low values of density. The fact that two of the lines ($\lambda 3889$ and $\lambda 7065$) have negative exponents in the temperature term does not provide as much leverage on the temperature because these two lines are also strongly affected by optical depth and collisional excitation effects.

Finally, for a more robust determination of the uncertainties in the physical parameters and ultimately in \bar{y} , we perform a Monte-Carlo simulation of the data. Starting with the observational inputs and their stated uncertainties, we have generated a data set which is Gaussian distributed for the 6 observed He emission lines. From each distribution, we randomly select a set of input values and run the χ^2 minimization. The selection of data is repeated 1000 times. We thus obtain a distribution of solutions for n, a_{HeI}, τ , and T and we compare the mean and dispersion of these distributions with the initial solution for these quantities.

In simple photoionization models, HII regions divide into two different ionization zones where the cooling is dominated by either O^+ or O^{++} . Typical abundance analyses usually take this into account and derive different electron temperatures for the two different zones (and use the

different electron temperatures for deriving ionic abundances, see Garnett 1992). In our new code we have the option of using two different temperatures in determining the He/H abundances (as done in PPR00 and LPPC, but not in IT98). We have experimented with this option, and, for this study have decided to concentrate on single temperature models. Given the number of physical parameters that one is solving for and the limited number of emission lines measured with high precision, satisfactory results were only achieved in cases where a relationship was assumed between the temperatures in the low and high ionization zones (as is usually done when calculating oxygen abundances). Since we are advocating non-parametric solutions, we felt it best to stick to the simpler case of single temperature solutions.

3. Revisiting NGC 346 from PPR00

The study of NGC 346 by PPR00 emphasized the advantages (relative to studying more distant blue compact galaxies) of (1) no underlying absorption correction for the helium lines, (2) the opportunity to observe multiple lines of sight, and (3) due to a lower electron temperature, the effects of collisional excitation on the permitted lines are small. They also identified the disadvantage of a larger correction for chemical evolution for the study of the primordial helium abundance. This study introduced the technique of deriving the electron temperature directly from the helium lines. Given the high quality of observations presented there, it is a good starting point to compare our own analysis techniques. Here we will concentrate on their region “A”, which provides the highest quality spectrum. The relevant He I emission lines, equivalent widths, and errors, taken from PPR00, are presented in Table 1. Here we have taken the reddening corrected He I emission line fluxes and their associated errors directly from PPR00. In analyzing these data, our main goal is to see if our analysis is consistent with that of PPR00.

In OS we made specific suggestions about treating the errors in the reddening correction, and we thought it would be interesting to revisit that question here. Thus, we carry out parallel analyses on a second set of data. The second set of data listed in Table 1 (labeled “re-analyzed”) have been derived from the original flux ratio observations of PPR00 and then de-reddened using the prescription for solving for reddening and underlying H absorption as described in OS. For this second set, we have adopted the average extinction law of Cardelli, Clayton, & Mathis (1989; hereafter CCM). This is the most commonly used astrophysical extinction law, but it differs slightly from that of the normal extinction law of Whitford (1958) used by PPR00. Since the extinction law is normally assumed without any associated errors, we were interested in the effect of simply

using a different (although generally acceptable) extinction law. Figure 2 shows the differences between the CCM extinction law and that used by PPR00. We also assign errors of 10% to the EW measurements (as some value of error is needed for our minimization technique, and none is reported in PPR00). The error in the EW is a conservative one, but the final results do not change significantly if the errors are varied between 10% and 2%.

In what follows we refer to a simple minimization based on the input data as a “direct” analysis (labeled “D” in the tables), and an analysis over 1000 representations which are consistent with the errors in the input data as a “Monte Carlo (“MC”) analysis.” In our first analysis, we assume a temperature of 11,920 K, the average He I temperature found by PPR00. Holding this temperature fixed, and assuming no underlying absorption, we derive values of $\text{He}^+/\text{H}^+ = 0.0795 \pm 0.0005$ and $n_e = 164_{-47}^{+56}$ which compare quite well with 0.0793 ± 0.0006 and 146 ± 50 reported by PPR00 (see Table 2). Dropping the assumption of zero underlying absorption gives a very similar result in the direct analysis, supporting PPR00’s claim that there is no underlying absorption (see Table 2). Using a Monte Carlo analysis, we derive $\text{He}^+/\text{H}^+ = 0.0801 \pm 0.0011$ and $n_e = 159 \pm 69$, where we see that the central values are only slightly changed, but the error bars on He^+/H^+ increase by about a factor of two (see Table 2). The close similarity of the two results indicates that our minimization techniques produce similar results with high quality data and similar assumptions. Although the PPR00 could not use the radiative transfer results of Benjamin Skillman, & Smits (2002), the spectrum for NGC 346 indicates very low values of $\tau(3889)$, so good agreement is expected.

In Figure 3, we show the results of our analysis for the case where we have fixed the temperature and allow for positive values of the underlying absorption coefficient, a_{HeI} . For this model we have used a two zone temperature model and assumed that the temperatures in those two zones are identical to the values derived by PPR00. Thus, the main difference between these calculations and those of PPR00 are dropping the assumptions of zero underlying absorption and zero optical depth in the triplet helium lines. Note the very good agreement between the our results (shown by the position of the solid circle) and those of PPR00 (shown by the intersection of the vertical and horizontal lines). The small dots show the possible variations in solutions due to the Monte Carlo generation of data. The solid square shows the position of the mean value of the 1000 sets of generated data. While the mean value is consistent with both our direct solution and PPR00, the uncertainty in y^+ is nearly doubled.

When we allow the code to solve for the electron temperature, we get a slightly higher value of

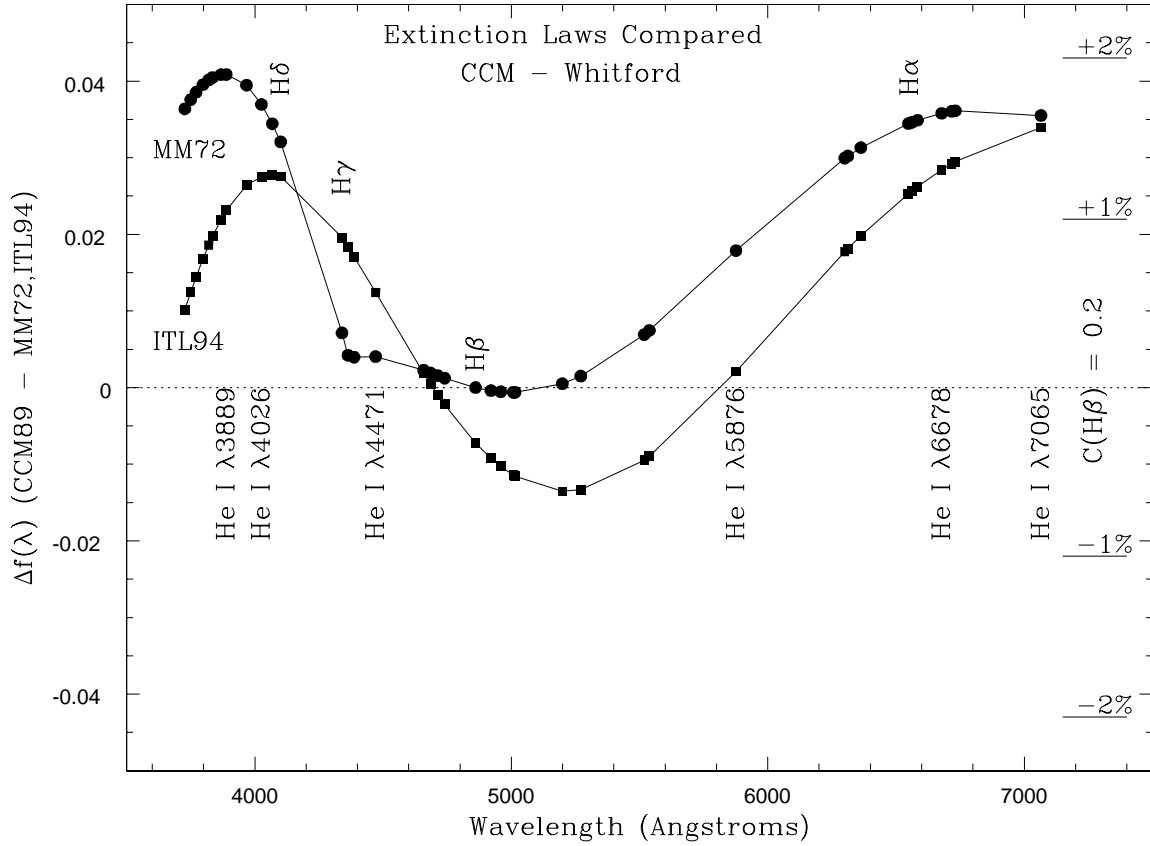


Fig. 2.— Comparisons between the extinction law of Whitford (1958) (as parameterized by Miller & Mathews 1972 - MM72 - and Izotov, Thuan, & Lipovetsky 1994 - ITL94) and the extinction law of Cardelli, Clayton, & Mathis (1989). The curves show points for major HII emission lines. The horizontal lines in the right of the figure show the resultant differences in dereddened emission line strengths for a logarithmic reddening at $H\beta$ of 0.2, which is typical of the extragalactic HII regions observed for helium abundance studies.

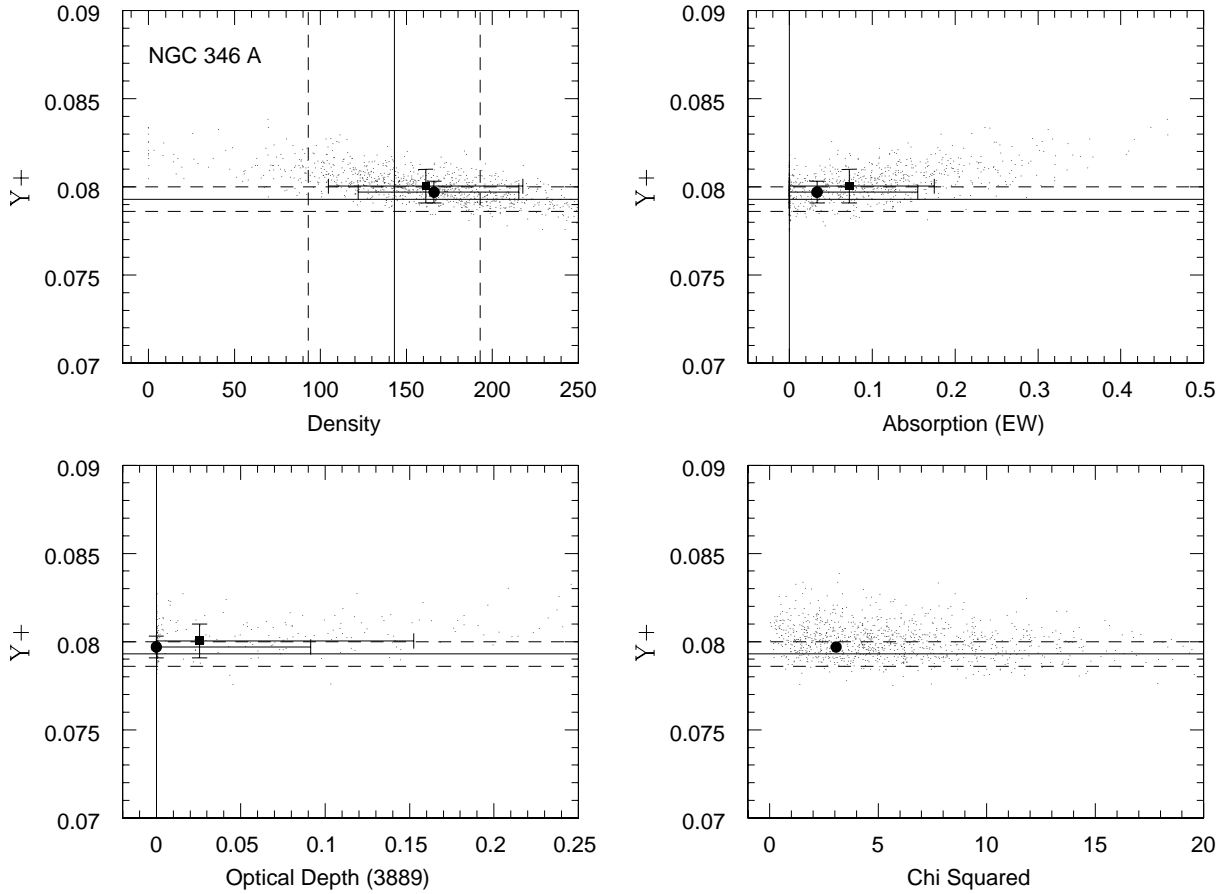


Fig. 3.— Results of modeling of 6 He I line observations of NGC 346 from Peimbert et al. (2000; PPRO0). The solid lines show the values derived by PPR00 and the dashed lines show the 1σ errors on those values. The solid circles (with error bars) show the results of our χ^2 minimization solution (with calculated errors). The small points show the results of Monte Carlo realizations of the original input spectrum. The solid squares (with error bars) show the means and dispersions of the output values for the χ^2 minimization solutions of the Monte Carlo realizations.

12,510 K (see Table 2). This temperature lies between the values of T(O III) (13,070 K) and T(O II) (11,810 K), which would normally be expected (Peimbert, Peimbert, & Luridiana 2002). This new solution drops the χ^2 value from 3.0 to 2.4, which an *ftest* shows is significant only at the 45% confidence level. The solution with the higher temperature also favors a lower density and a small amount of underlying absorption (although consistent with zero) with a resulting He^+/H^+ ratio which is 2% higher than the PPR00 value. Note that, although 2% seems like a small difference, the value obtained from the direct analysis allowing for underlying absorption and deriving the electron temperature from the helium line ratios is 3σ higher than the PPR00 value. The MC value is slightly higher still, but this could be mainly due to the fact that the code requires the underlying absorption to be positive, so that, when the value is close to zero, there is a bias in the mean value to be larger. The results of the MC analysis are shown in Figure 4. In addition to the value of y^+ being larger, the uncertainty in y^+ is now over a factor of 2 larger than quoted in PPR00.

As a check on the assumption of positive underlying He absorption, we then ran the direct and Monte Carlo codes allowing both positive and negative values of underlying He absorption. The result of the direct analysis is almost identical to that obtained with the absorption held positive (see Table 2). In the table, ‘solved +’ refers to the restriction that only positive values of the parameter were permitted, ‘solved free’ indicates that both positive and negative values are allowed, and ‘fixed’ means that the parameter was not solved for, but rather an input value was used and held fixed. Thus, the detection of a small amount of underlying He absorption is not due to a bias from the code only allowing positive values. The higher values of the He abundance (roughly 2% higher for the direct method and 3% higher for the Monte Carlo method) are probably due to a small, but real, amount of underlying He absorption.

Finally we ran the direct and Monte Carlo codes allowing both positive and negative values of all three physical parameters: density, underlying absorption, and optical depth while still solving for electron temperature (last lines in Table 2). Note that negative values of density and optical depth are non-physical. Now the favored value for the underlying absorption is almost very close to zero. However, it is very interesting that the free solution has favored negative (non-physical) values of the optical depth. In this solution, because of the negative value for the optical depth, the density has jumped up to 427 (mainly because of the inverse dependences on density and optical depth for the $\lambda 7065$ line), resulting in a He^+/H^+ value which is even lower than the PPR00 value. The favored negative values of the optical depth indicate that either our prescription for the treatment of radiative transfer on the helium line strengths is not appropriate for NGC 346 or that

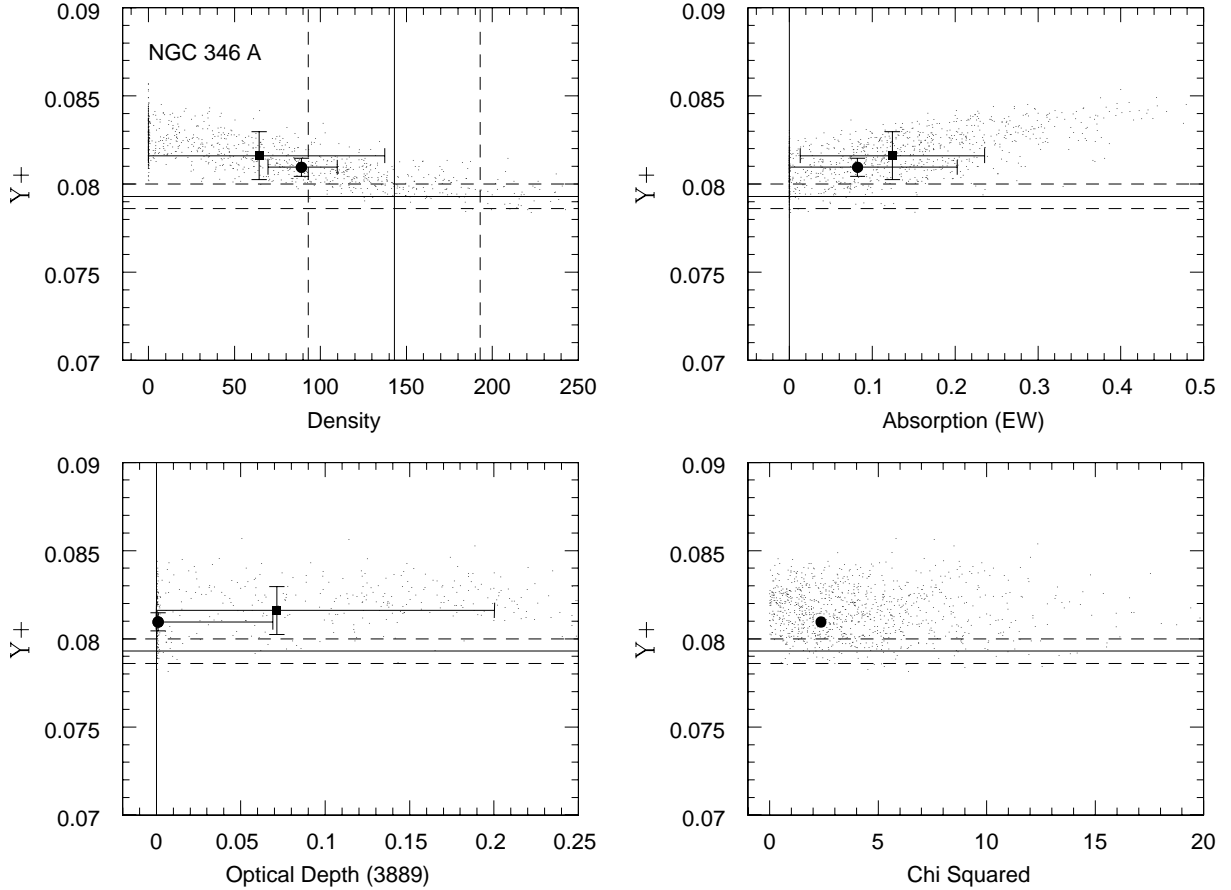


Fig. 4.— As in Fig. 3, but we have assumed a single temperature and solved for that temperature. Here, larger values of absorption and lower values of density result in higher values of He/H. The solid lines show the values derived by PPR00 and the dashed lines show the 1σ errors on those values. The solid circles (with error bars) show the results of our χ^2 minimization solution (with calculated errors). The small points show the results of Monte Carlo realizations of the original input spectrum. The solid squares (with error bars) show the means and dispersions of the output values for the χ^2 minimization solutions of the Monte Carlo realizations.

the value for $\lambda 3889$ (the main driver of the optical depth solution) is somewhat in error (or both).

From this exercise we conclude that the error bars on the derivation of individual HII region parameters are underestimated for several reasons. First, as concluded in OS, unless a Monte Carlo analysis of the data is performed, the resulting errors of a single minimization exercise are likely to be underestimates. In the case for which we solve for temperature and absorption, our MC uncertainty is over a factor of 2 larger than that quoted by PPR00. Second, by making different reasonable assumptions, different central values of the helium abundance are obtained (and these values differ by several standard deviations if the errors are calculated in the direct manner). For NGC 346A these differences are only a few percent because the quality of the data constrains the results to a relatively narrow range. However, typical HII region spectra used for deriving helium abundances are not even close to the quality of the NGC 346A spectrum from PPR00. Third, by allowing the code to examine non-physical values of certain parameters there is an indication that perhaps the prescription for treating the radiative transfer is not completely appropriate. This implies a systematic uncertainty which has not been accounted for in the errors analysis.

In Table 2 we also report the results of re-analyzing the NGC 346A spectrum using our favored prescriptions for the solution for reddening and underlying hydrogen absorption and the appropriate error propagation (we label these entries “re-an”). Our analysis finds a similar value for $C(H\beta) = 0.174 \pm 0.008$ (compared to 0.15 ± 0.01 for PPR00), and no evidence of underlying hydrogen absorption (formally $-0.6 \pm 0.5 \text{ \AA}$). As seen in Table 1, there are small differences between the PPR00 relative line fluxes and those resulting from our re-analysis, which are mostly due to the differences in the adopted reddening curve (and some small differences might be expected simply due to round-off errors). As expected, only small differences are found when we analyze these helium ratios (as shown in Table 2). There is, however, one interesting difference. When we solve for all of the parameters including temperature, the temperature is higher (although not as high as the [O III] temperature) with the result that the density falls and the helium abundance rises by 2% relative to that found in the similar analysis with the PPR00 data. Both the original data and the re-analyzed data favor negative values of the optical depth. It appears that even with excellent quality spectra, one is never far from unsatisfactory results, and that one needs exquisite quality data to insure that the best minimization values favor physically meaningful values.

A detailed inspection of Table 2 indicates that the values derived for the physical parameters and the helium abundance depend on the assumptions that are made in the analysis. While the variations are of order 2 – 3% for most of the helium abundance determinations, this is very

significant for determination of η , and of order the discrepancies found in the literature. For example, the PPR00 value of $y^+ = 0.0793$ corresponds to a ${}^4\text{He}$ mass fraction of 0.2403, from which they inferred a primordial abundance of 0.2345 which in turn corresponds to $\eta_{10} = 1.9$. Our value (using the re-analyzed data) of $y^+ = 0.0828$ corresponds to a ${}^4\text{He}$ mass fraction of 0.2483. Using the same slope (dY/dZ) yields a primordial abundance of 0.2425 which in turn corresponds to $\eta_{10} = 3.5$. Thus, one sees a difference of nearly a factor of two in the derived value of η_{10} simply from using a different set of assumptions.

Figure 5 underscores this point. Here we have plotted the He^+/H^+ ratios and errors derived for each line as a result of our direct method which solves simultaneously for helium abundance, temperature, density, underlying absorption and optical depth under the assumption that all are positive. The solid and dotted lines across the bottom indicate the solution from PPR00. The significant difference is due primarily to assumptions made in analyzing the observations. In other words, an independent analysis, using reasonable assumptions, produces a value of $\text{He}^+/\text{H}^+ = 0.0828 \pm 0.0008$, which is over 4% (or 6σ) higher than the PPR00 value. We are not claiming here that this solution is superior to that produced by PPR00, only that it is a completely satisfactory solution but different. These systematic differences need to be accounted for in estimating errors in the final helium abundance.

What is the “best” value for He^+/H^+ in NGC 346A? We favor an estimation which is as close to a non-parametric solution as possible. Thus, we feel that solving for electron temperature from the helium lines and allowing only for non-negative values of underlying absorption is preferred². This is not a truly non-parametric solution as we are still dependent on assumptions concerning the relative importance of underlying helium absorption and optical depth on the different helium lines. For our analysis of the PPR00 data for NGC 346A, this means that we favor 0.0828 ± 0.0008 , which, compared with the result of PPR00 (0.0793 ± 0.0006) appears extremely high, and would even appear to rule out their value. At this point we are not ready to interpret the results in that way. Our main conclusion is that the systematic error of analysis technique is clearly dominant, and that this error, when reported, has been grossly underestimated in the past.

²If the underlying absorption is negative, then our assumption that it is roughly equal at all wavelengths is no longer true. That is one of the reasons we also search for solutions where a_{HeI} (as well as the other parameters) is allowed to be negative.

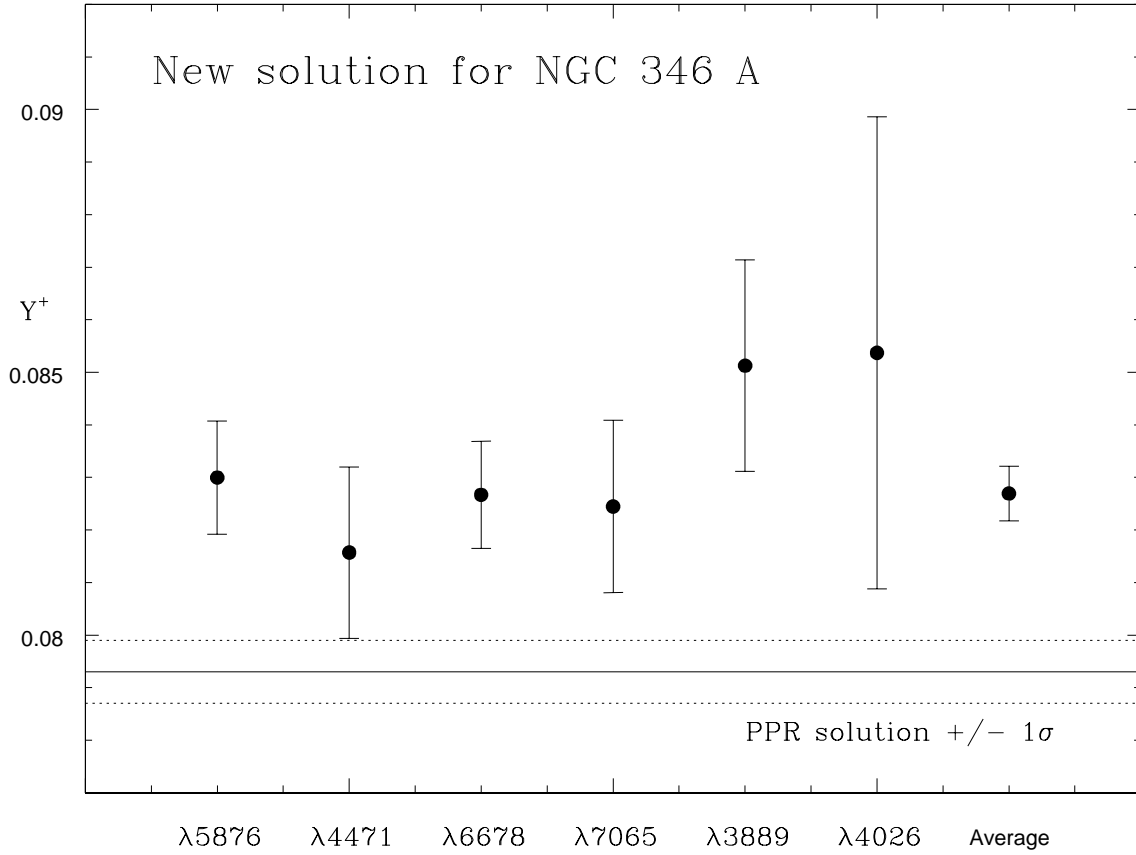


Fig. 5.— Results of modeling of 6 He I line observations of NGC 346 A from Peimbert et al. (2000; PPRO0). Here we show the He^+/H^+ ratios and errors derived for each line as a result of our direct method which solves simultaneously for helium abundance, temperature, density, underlying absorption and optical depth under the assumption that all are positive. The solid and dotted lines across the bottom indicate the solution from PPR00. The significant difference is due primarily to assumptions made in analyzing the observations.

4. Revisiting Select Targets from IT98

It is now useful to revisit selected targets from IT98 to better assess the robustness of their results. Many of the targets in IT98 are not of the quality necessary for high accuracy helium abundance determinations. For example, the majority are not of sufficient quality to detect the $\lambda 4026$ line which provides a strong constraint on the underlying He I absorption. Thus, we have chosen to re-analyze only a select few targets which meet three criteria. First we select only the IT98 targets with $EW(H\beta) \geq 200\text{\AA}$. This cut is made in order to minimize the correction due to underlying absorption as well as to improve the signal-to-noise ratio in faint lines such as $\lambda 4026$ (the PPR00 value of $EW(H\beta)$ for NGC 346A is 250). The value of 200\AA is identified by Izotov & Thuan (2004; IT04) as a desirable cut-off. This selection screens out 35 of the 45 IT98 spectra. Next we select targets with oxygen abundances less than 20% of the solar value (4.6×10^{-4} ; Asplund *et al.* 2004). This cut minimizes the uncertainty induced by our lack of knowledge of the functional form of the relationship between ^4He and O/H (c.f., Olive, Steigman, & Walker 1991; Pilyugin 1993; Carigi et al. 1995; Bradamante, Matteucci, & D’Ercole 1998; Fields & Olive 1998). This selection screens out 17 of the 45 IT98 spectra. Finally we select out targets with radial velocities inside of the ranges $728 \pm 100\text{ km s}^{-1}$ and $1032 \pm 100\text{ km s}^{-1}$ (to avoid contamination of He I $\lambda 5876$ by Na I absorption; cf. Dinerstein & Shields 1986). This selection screens out 10 of the 45 IT98 spectra. Clearly several of the targets fail more than one of the screens. In the end, we find there are seven targets which pass all three screens, and hereafter we will refer to this subsample as the “high quality” sample.

We proceed in the same manner as our analysis of NGC 346A, i.e., we analyze the reported reddening corrected He I line strengths directly and also re-analyze the data starting from the raw flux ratio measurements. For our analysis, we require the EW of the He I lines. In most cases these are not reported, so we have estimated the strength of the continuum (from published spectra) and used the $EW(H\beta)$ to derive these EWs. This is, of course, less than desirable, and, at first, we hesitated to carry this out. However, since the primary effect is on the value of the underlying absorption, and since it is the ratio of the lines strengths that matters here, it turns out that the answers have a relatively low sensitivity to these estimated values. We assigned uncertainties to the estimated EW of 10%. In fact, changes of these values of up to 20%, in most cases, have little effect on the derived helium abundances. In cases where we have re-analyzed the data by deriving our own reddening and underlying absorption corrections, we have also estimated the EW of the Balmer lines in the same way.

4.1. SBS 0335-052

A spectrum for SBS 0335-052 was reported in IT98 (and therefore we do not need to make any adjustments to be consistent with the IT98 analysis as will be the case for other targets). When we re-analyze the IT98 spectrum for SBS 0335-052 using our favored prescriptions for the solution for reddening and underlying hydrogen absorption, we obtain a value of $C(H\beta) = 0.121 \pm 0.014$, in good agreement with IT98 value of 0.13, and we find a higher value for the underlying hydrogen absorption of $1.3 \pm 0.9 \text{ \AA}$ (to be compared with IT98 value of 0.4 \AA). The resulting helium line strengths are reported in Table 3. There are only small differences between the IT98 values and the values resulting from our re-analysis. The one noticeable difference is for $\lambda 3889$, where our value is 9% higher due primarily to the correction for underlying H absorption.

Table 4 shows the the results of the full set of analyses of the IT98 spectrum for SBS 0335-052. Our constrained analyses with the assumption of no underlying He absorption find much higher values of the optical depth in the in helium lines (≈ 5 vs. 1.7) and this results in lower densities but almost no difference in the value of the He abundance. However, when we allow for underlying absorption, there is significant evidence for this and this results in higher helium abundances. The χ^2 drops significantly with the allowance for underlying absorption and the helium abundance rises significantly. Given the large variation in helium abundance values for the different degrees of constraint, it would appear that this spectrum of SBS0335-052 is not suitable for constraining the primordial helium abundance.

By solving for the temperature, significantly lower temperatures (with significantly larger uncertainties) and higher densities are found, with the resultant much lower He abundances. The derived temperatures are so much lower than the [O III] temperatures such that these solutions are most likely not to be believed. The very high values of $\tau(3889)$ are robust, and it is unlikely that our prescription for correcting for optical depth effects is valid in this regime.

Although SBS 0335-052 is an ideal target from the viewpoint of its exceptionally low O/H abundance, the very high value of optical depth means that this is probably a less than suitable object (at least in the highest surface brightness knot) for determining helium abundance. This is reflected in the fact that the error in He^+/H^+ in SBS 0335-052 is the largest (in both absolute terms and relative terms) of the seven objects from IT98 that we have re-analyzed.

4.2. NGC 2363A

The spectrum for NGC 2363A analyzed in IT98 was first reported in Izotov, Thuan, & Lipovetsky (1997; ITL97). In ITL97, an electron temperature of $15,100 \pm 100$ K, an oxygen abundance of $0.78 \pm 0.01 \times 10^{-4}$, and a helium abundance of $Y = 0.245 \pm 0.005$ were reported. IT98 re-analyzed this spectrum, and, primarily because of a difference in the estimated electron temperature, the oxygen abundance changed to $0.71 \pm 0.01 \times 10^{-4}$ (a 7σ decrease), and the helium abundance changed to $Y = 0.2456 \pm 0.0008$ (an 84% decrease in the uncertainty). That such different values can be reported from the same spectrum by the same researchers gives one an impression of the size of the systematic errors. For our comparison analysis, we will assume an [O III] electron temperature of $15,800 \pm 100$ K, which would correspond to the scale used in IT98.

When we re-analyze the IT98 spectrum for NGC 2363A using our favored prescriptions for the solution for reddening and underlying hydrogen absorption, we obtain a value of $C(H\beta) = 0.117 \pm 0.003$, in good agreement with the ITL97 value of 0.11, and we find a slightly lower value for the underlying hydrogen absorption of $1.4 \pm 0.3 \text{ \AA}$ (to be compared with ITL97 value of 1.8 \AA). The resulting helium line strengths are reported in Table 3. There are only small differences between the IT98 values and the values resulting from our re-analysis (all consistent with round-off errors).

Table 5 shows the results of our analyses of the HeI line ratios. In all analyses where their presence is allowed, we find evidence for significant amounts of underlying absorption and optical depth effects (which were both assumed to be absent in the IT98 analysis). Holding the electron temperature fixed at the [O III] temperature and assuming no underlying absorption reveals values of $\tau(3889) \approx 2$. When underlying absorption is allowed for, the solutions favor significant amounts (the χ^2 drops by a factor of 6). Finally, solving for the electron temperature yields a lower temperature. Note that the value of the derived helium abundance varies by 8% depending on the set of assumptions used in the derivation. Perhaps the most remarkable thing about this re-analysis is that our value derived by allowing for underlying absorption and optical depth effects and solving for the temperature produces a value nearly identical to the IT98 value although our uncertainty (from the MC analysis) is 4.6 times larger.

4.3. SBS 0940+544N

The spectrum for SBS 0940+544N analyzed in IT98 was reported in ITL97. In ITL97, an electron temperature of $19,000 \pm 300$ K, an oxygen abundance of $0.30 \pm 0.01 \times 10^{-4}$, and a helium

abundance of $Y = 0.246 \pm 0.008$ were reported. IT98 re-analyzed this spectrum, and, primarily because of a difference in the estimated electron temperature, the oxygen abundance changed to $0.27 \pm 0.01 \times 10^{-4}$, and the helium abundance changed to $Y = 0.2500 \pm 0.0047$. For our comparison analysis, we will assume an [O III] electron temperature of $20,200 \pm 300$ K, which would correspond to the scale used in IT98.

When we re-analyze the IT98 spectrum for SBS 0940+544N using our favored prescriptions for the solution for reddening and underlying hydrogen absorption, we obtain a value of $C(H\beta) = 0.048 \pm 0.023$, in good agreement with the ITL97 value of 0.05, but, formally, we find a negative value (though consistent with 0) for the underlying hydrogen absorption of $-1.4 \pm 1.4 \text{ \AA}$ to be compared with ITL97 value of 0.6 \AA . This presents a problem concerning how to proceed with the analysis. Since the solution is formally consistent with no underlying absorption, we assume a value of $0 \pm 1.4 \text{ \AA}$ in our analyses. The resulting helium line strengths are reported in Table 3. There are only small differences between the IT98 values and the values resulting from our re-analysis (all consistent with round-off errors).

Table 6 shows the results of our analyses of the HeI line ratios. Our analyses are generally in agreement with IT98 in that low values of underlying absorption, optical depth, and density are found. However, perhaps the most interesting part of our re-analysis can be seen when non-physical values are allowed for. Specifically, negative values of underlying absorption and optical depth are favored. These non-physical values indicate that there must be some problem with either the spectrum or our simple assumptions used when analyzing it.

4.4. MRK 193

The spectrum for MRK 193 analyzed in IT98 was first reported in ITL94. In ITL94, an electron temperature of 15,500, an oxygen abundance of $0.70 \pm 0.02 \times 10^{-4}$, and a helium abundance of $Y = 0.253 \pm 0.007$ were reported. IT98 re-analyzed this spectrum, and, primarily because of a difference in the estimated electron temperature, the oxygen abundance changed to $0.64 \pm 0.01 \times 10^{-4}$, and the helium abundance changed to $Y = 0.2478 \pm 0.0037$. For our comparison analysis, we will assume an [O III] electron temperature of $16,200 \pm 200$ K, which would correspond to the scale used in IT98.

When we re-analyze the IT98 spectrum for MRK 193 using our favored prescriptions for the solution for reddening and underlying hydrogen absorption, we obtain a value of $C(H\beta) = 0.292 \pm$

0.020, in good agreement with the ITL94 value of 0.260, but, formally, we find a negative value for the underlying hydrogen absorption of $-1.7 \pm 1.0 \text{ \AA}$ (to be compared with ITL94 value of 1.9 \AA). As in the case of SBS 0940+544N, this again presents a problem concerning how to proceed with the analysis. In this case, the solution is not formally consistent with zero underlying absorption, but we are forced to assume a value of $0 \pm 1.0 \text{ \AA}$ in our analyses. The resulting helium line strengths are reported in Table 3. There are only small differences between the IT98 values and the values resulting from our re-analysis, except for the difference in $I(\lambda 3889)$.

Table 7 shows the results of our analyses of the HeI line ratios. Our analyses are generally in agreement with IT98 in that low values are found for underlying absorption and relatively high densities of density. However, non-zero values of optical depth are favored, and strongly so in the re-analyzed data. When the temperature is solved for, lower values are favored. Overall, once again the impression is that the assumptions of the analysis strongly affect the derived value of Y .

4.5. SBS 1159+545

The spectrum for SBS 1159+545 analyzed in IT98 was first reported in ITL94. IT98 re-analyzed this spectrum upon discovering errors made in the data reduction reported in ITL94. Since the full spectrum and analysis for SBS 1159+545 was reported in IT98 we do not need to make any adjustments for consistency. When we re-analyze the IT98 spectrum for SBS 1159+545 using our favored prescriptions for the solution for reddening and underlying hydrogen absorption, we obtain a value of $C(H\beta) = 0.065 \pm 0.016$, in good agreement with the IT98 value of 0.06, and we find a value for the underlying hydrogen absorption of $0.2 \pm 1.1 \text{ \AA}$ (smaller than but consistent with the IT98 value of 0.6 \AA). The resulting helium line strengths are reported in Table 3, and, in general, there is very good agreement.

Table 8 shows the results of several analyses of the IT98 spectrum for SBS 1159+545. When we fix the temperature to the IT98 value and assume no underlying He absorption, we find a value of the helium abundance consistent with that of IT98 and also an optical depth of zero, consistent with IT98. Interestingly, when we re-analyze the spectrum, the helium line strengths change only slightly, but even in the constrained analysis, the favored density has fallen, the optical depth is non-zero, and the favored helium abundance has risen by 2% (while the χ^2 is almost identical).

In the constrained solutions, there is never any evidence of underlying He absorption in the SBS 1159+545 spectrum. The less constrained solutions show why. There, negative values of

underlying absorption are strongly favored. Indeed, in the unconstrained solutions, negative values for both underlying He absorption and optical depth are favored, resulting in very high values of density, relatively low values of temperature, and thus, unrealistically low values of the He^+/H^+ ratio. Although the SBS 1159+545 spectrum is fairly high signal/noise, it would appear that a robust measurement of the helium abundance may be suspect for this spectrum.

4.6. Haro 29

The spectrum for Haro 29 analyzed in IT98 was reported in ITL97. In ITL97, an electron temperature of $15,400 \pm 100$ K, an oxygen abundance of $0.65 \pm 0.01 \times 10^{-4}$, and a helium abundance of $Y = 0.246 \pm 0.005$ were reported. IT98 re-analyzed this spectrum, and, primarily because of a difference in the estimated electron temperature, the oxygen abundance changed to $0.59 \pm 0.01 \times 10^{-4}$, and the helium abundance changed to $Y = 0.2509 \pm 0.0012$. For our comparison analysis, we will assume an [O III] electron temperature of $16,180 \pm 100$ K, which would correspond to the scale used in IT98.

When we re-analyze the IT98 spectrum for Haro 29 using our favored prescriptions for the solution for reddening and underlying hydrogen absorption, we obtain a value of $C(\text{H}\beta) = 0.001 \pm 0.004$, in good agreement with ITL97 value of 0.0, and we find a value for the underlying hydrogen absorption of $2.7 \pm 0.3 \text{ \AA}$ (to be compared with IT98 value of 2.5 \AA). The resulting helium line strengths are reported in Table 3, and, in general, there is very good agreement.

Table 9 shows the the results of several analyses of the IT98 spectrum for Haro 29. Our constrained analyses with the assumption of no underlying He absorption find evidence for non-zero optical depth in the in Helium lines and this results in higher densities and thus, lower values of the He abundance. However, when we allow for underlying absorption, there is very significant evidence (the χ^2 drops roughly a factor of 6 with the allowance for underlying absorption) and this results in higher helium abundances. When we solve for the temperature, the value is very close to that obtained from the [O III] lines, which is reassuring, and the solutions do not change significantly when we allow for positive or negative values for the underlying absorption. However, for our least constrained solutions, we find the very discouraging result that very different solutions are found with higher values of the optical depth, higher values of the underlying He absorption, negative densities, higher electron temperatures and very high helium abundances. The slightly lower χ^2 for these solutions are probably only a warning of how loosely constrained even the best solutions are.

LPPC03 have analyzed the IT98 spectrum of Haro 29 and derive a value of $\text{He}^+/\text{H}^+ = 0.078$. There are two large differences between their treatment and the one presented here. First, a much larger value of the reddening is adopted and second, underlying He absorption is assumed to be zero. In all of our solutions, we find this to be a poor assumption.

4.7. SBS 1420+544

A spectrum for SBS 1420+544 was reported in IT98 (and therefore we do not need to make any adjustments to be consistent with the IT98 analysis as for most of the targets). When we re-analyze the IT98 spectrum for SBS 1420+544 using our favored prescriptions for the solution for reddening and underlying hydrogen absorption, we obtain a value of $C(\text{H}\beta) = 0.167 \pm 0.013$, in good agreement with IT98 value of 0.16, and we find a value for the underlying hydrogen absorption of $0.4 \pm 0.9 \text{ \AA}$ (to be compared with IT98 value of 0.0 \AA). The resulting helium line strengths are reported in Table 3, and, in general, there is very good agreement with the IT98 values.

Table 10 shows the the results of several analyses of the IT98 spectrum for SBS 1420+544. SBS 1420+544 is interesting in that it is one of the few HII regions for which IT98 find definite signs of significant optical depth. Our constrained solutions with underlying absorption fixed at zero find higher values for the optical depth, and this results in larger values of the density and lower values of the He^+/H^+ ratio. When we allow for underlying He absorption, there is only weak or no evidence of this. However, when we allow for the temperature to be solved for, significantly larger temperatures result, giving lower densities and higher helium abundances. Using our re-analyzed spectrum and solving for temperature, the resulting helium abundance is significantly higher (by 4%) than IT98.

Given the evidence for the large optical depth in the helium lines, and the large uncertainty in our prescription for correcting for this, it would seem that again, a robust measurement of the helium abundance is difficult for this spectrum.

4.8. Summary of Re-analysis of IT98 Spectra

A summary of our re-analysis of the IT98 spectra is given in Table 11. Several differences between the results of the IT98 analysis and our re-analysis are immediately apparent. First, the physical parameters T , N , $\tau(3889)$, and $\text{He}(\text{ABS})$ are all significantly less well constrained in our

re-analysis. In some cases, this is because some of these values were assumed to be zero with no associated errors, and in other cases we believe that the errors were underestimated. The larger uncertainties in the physical parameters naturally translate into larger uncertainties in the helium abundances.

Table 11 shows a larger dispersion in the re-analyzed He abundances, with a slight bias toward higher values. Note that in the discussions of the individual objects we raised reservations concerning the suitability of several of these spectra for deriving very high accuracy helium abundances. Specifically, SBS 0940+544N and MRK 193 both favored negative (non-physical) values for underlying hydrogen absorption. SBS 0335-052 and SBS 1420+544 both have relatively large values of $\tau(3889)$, and we doubt that the simple prescription for correcting for optical depth effects will be accurate in this regime. Although we specifically selected objects with high emission line equivalent width, two objects (NGC 2363 A and Haro 29) show significant evidence for underlying helium absorption, and thus, are dependent on our assumption of the behavior of the absorption equivalent widths on a line-by-line basis.

In sum, even the spectra that were selected specifically to be the highest quality provide only nominal constraints on the physical conditions in the HII regions, and thus, carry significant errors on their helium abundances compared to what is necessary to constrain the value of the primordial helium abundance.

5. Revisiting Select Targets from IT04

Recently, Izotov & Thuan (2004; IT04) have presented new observations of 33 HII regions in order to provide a better metallicity baseline and therefore stronger constraints on dY/dZ . They combine these new observations with those of IT98 to conduct an analysis of 82 HII regions. We have studied the new spectra presented by IT04 to determine if there are new observations which satisfy our criteria for inclusion in a “high quality” data sample, and, in fact, there are seven targets that do satisfy the criteria enumerated at the beginning of §4. These seven targets, in order of increasing metallicity are: J 0519+0007, HS 2236+1344, HS 0122+0743, HS 0837+4717, CGCG 007-025, HS 0134+3415, and HS 1028+3843. We performed a complete analysis of these seven targets following the method used in §4.

Unfortunately, we discovered a serious problem with many of the observations reported in IT04, which render them questionable for use in our analyses. When we solve for the reddening and

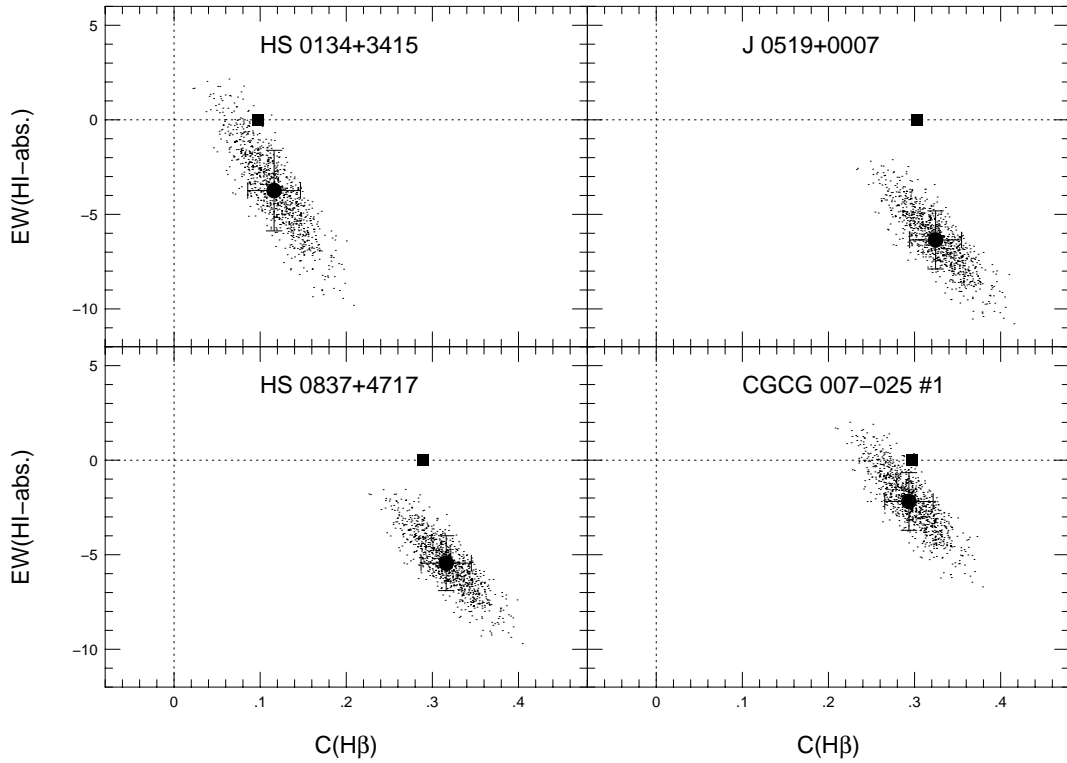


Fig. 6.— Solutions for the value of reddening, $c(H\beta)$, and underlying Balmer absorption, $EW(HI-abs.)$, for four of the “high quality” data points from IT04. In all four cases, we find that the “best” solution requires significantly negative values of $EW(HI-abs.)$ which is probably not physically realistic. The small points show the results of our Monte Carlo modeling and the large circles with error bars show our best values with errorbars. The square points are the solutions reported by and used by IT04.

underlying Balmer absorption in the spectra from IT04, we often encounter significantly negative values of underlying Balmer absorption. This is found in 4 of the 7 cases identified as potential “high quality” sample targets. Figure 6 shows the solutions for these four sources. The solutions for underlying absorption are found to be negative ranging from 1.4σ for CGCG 007-025 to 4.1σ for J 0519+0007. As can be seen from Figure 6, in all cases IT04 derived values of 0 \AA for the underlying Balmer ratios. This may be due to limiting the solution to physically meaningful, i.e., positive values.

As noted before, it was problematic that two of the targets in the IT98 “high quality” data sample showed negative values for underlying Balmer absorption (SBS 0940+544N at the 1.0σ level and Mrk 193 at 1.7σ), but the prevalence in the new sample cannot be ignored. In fact, roughly half of the new observations reported in IT04 indicate zero underlying Balmer absorption, indicating that this problem exists throughout the dataset. If we look at the object in the “high quality” data sample with the most negative value of underlying Balmer absorption (J 0519+0007) we find that the reddening corrected values for the blue Balmer lines are all significantly too high relative to the theoretical values (i.e., $H\gamma/H\beta$, $H\delta/H\beta$, $H9/H\beta$, and $H10/H\beta$ are $+4.4 \sigma$, $+5.1 \sigma$, $+0.4 \sigma$, and $+1.8 \sigma$ respectively). In fact, the values for the blue Balmer lines before reddening correction are all close to their theoretical values, indicating very low reddening to this target. Brief inspection of the other targets reveals a similar pattern, indicating that the problem may be solely with the $H\alpha$ line (in the sense that the $H\alpha$ line is too strong) and this could point to a problem with the sensitivity calibration in that wavelength range. On the other hand, J 0519+0007 is at a Galactic latitude of -20° and according to Schlegel et al. (1998) should have an extinction of $A_V \sim 0.4 \text{ mag}$. If there is no problem with the sensitivity calibration, then the effect could be due to atmospheric differential refraction (cf., Filippenko 1982) even though the object was observed at an airmass of 1.2. An alternative explanation could be that these spectra indicate the collisional enhancement of the $H\alpha$ (see discussion in Skillman & Kennicutt 1993), but it seems unlikely that we would see it in so many sources and not find a strong correlation with electron temperature.

Until this problem is solved, we have reservations concerning the inclusion of the spectra from IT04 in our study of the primordial helium abundance. In Table 12 we have reported our re-analysis of the “high quality” sample of IT04. Unfortunately, IT04 do not report their derived values for n and $\tau(3889)$ so direct comparisons are not possible, but it appears that many of the characteristics from Table 11 are also found in Table 12. In our analysis, several of the targets show relatively large values of $\tau(3889)$ and significant evidence for underlying HeI absorption.

6. Towards a Primordial ^4He Abundance

Given the different possible assumptions one can make regarding the treatment of the underlying absorption, optical depth, or temperature, one can justifiably wonder whether it is indeed possible to extract a reliable value of the primordial abundance of ^4He from these observations. It is our hope that by striving to free our solutions from as many parametric constraints as possible and by considering all identifiable sources of error that we can now produce a value of the primordial helium abundance with reasonable error estimates.

If we take our preferred solutions based on the re-analyzed data (where we use the Monte Carlo technique and solve for temperature and restrict all parameters to take positive values) for the seven “high quality” targets from IT98, then a regression of y^+ on O/H yields an intercept of:

$$Y_p = 0.2491 \pm 0.0091 \quad (5)$$

The corresponding value for the baryon-to-photon ratio is

$$\eta_{10} = 6.64^{+11.1}_{-3.82} \quad (6)$$

easily in good agreement with the CMB determination of η . Figure 7 shows a comparison between the original IT98 values and our re-analysis for the seven “high quality” targets. It also compares the results of the above regression with the original value obtained by IT98 for the full set of 45 targets. The error on Y_p derived above and shown in Figure 7 is 4.5 times larger than derived by IT98. One could argue that we should drop the two observations which yielded negative Balmer absorption. In this case, our regression for five points would yield, $Y_p = 0.2470 \pm 0.0114$. While the intercept has decreased slightly, the uncertainty has increased making the 1σ upper limit virtually identical.

Obviously, some of the increase in the error is due to the decrease in the sample size from 45 to 7, and some of the increase in the error is due to a larger error on the slope due to a smaller metallicity baseline. However, a good part of the increase in the error is due to the larger error on the individual points. Additionally, some of the decrease in the intercept error gained by extending the metallicity baseline to higher metallicities is misleading because it is dependent on the questionable assumption of a perfectly linear relationship between Y and O/H.

We can investigate the effect of limiting the sample size by including some of the IT04 data points. If we include the three “high quality” targets from IT04 which do not show evidence of negative underlying H I absorption, using all eight points which show no sign of negative H I

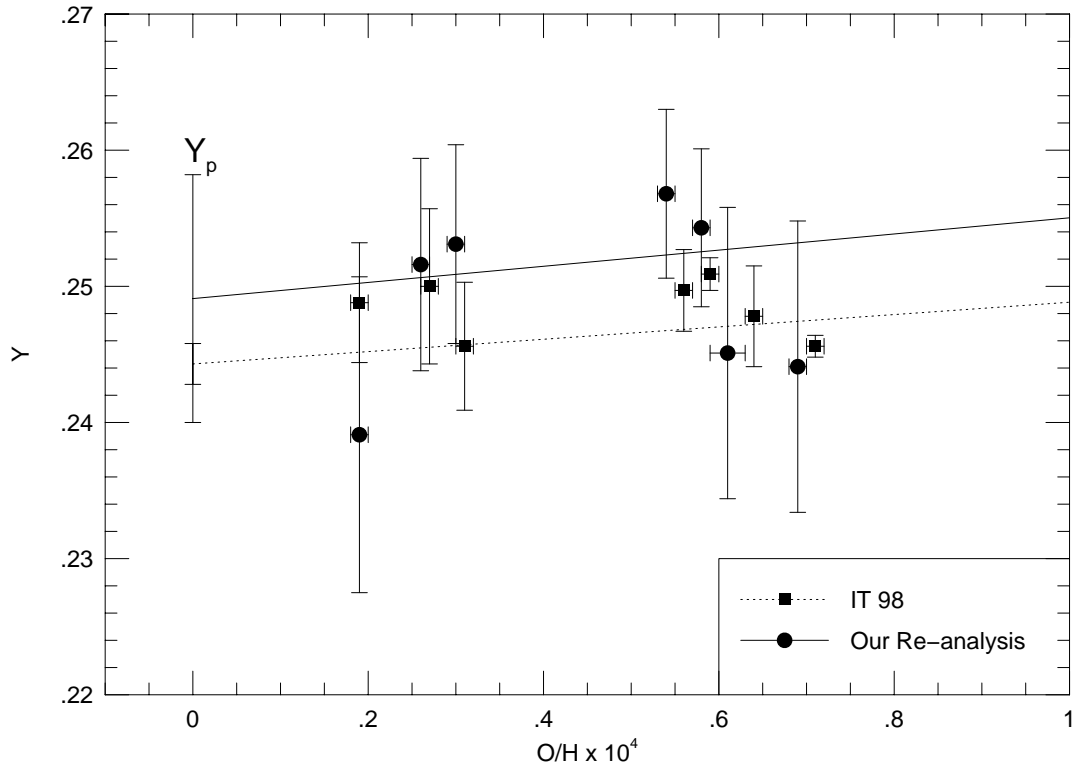


Fig. 7.— A comparison of the results for the best IT98 targets and our re-analysis of the spectra for those targets. The regression and the intercept with errors (Y_p) shown for IT98 is that resulting from the full sample of IT98 while the regression for the re-analysis is based on only the seven “high quality” targets.

absorption we obtain:

$$Y_p = 0.2502 \pm 0.0093 \quad (7)$$

The corresponding value for the baryon-to-photon ratio is

$$\eta_{10} = 7.48^{+12.9}_{-4.45} \quad (8)$$

again, easily in good agreement with the CMB determination of η . Finally, if we include all seven “high quality” targets from IT04 together with all seven from IT98, we obtain:

$$Y_p = 0.2504 \pm 0.0073 \quad (9)$$

The corresponding value for the baryon-to-photon ratio is

$$\eta_{10} = 7.63^{+9.1}_{-3.95} \quad (10)$$

also easily in good agreement with the CMB determination of η .

Note that although the error on Y_p is declining with the increase in number of targets, it is not decreasing as the square root of the number of targets. It appears that there is a floor in the uncertainty which is likely greater than 0.005.

In Figure 1 we summarize our view of the present situation. Clearly the true uncertainty on the primordial helium abundance is much larger than indicated in previous studies. We cannot rule out values as high as the those achieved with our re-analysis of the IT98 observations. Neither can we rule out values as low as those derived by PPR00. Thus, perhaps the best we can say is that the primordial ${}^4\text{He}$ abundance lies within the “conservative allowable range” indicated in Figure 1.

$$0.232 \leq Y_p \leq 0.258 \quad (11)$$

This extended range in Y_p corresponds to

$$1.8 \leq \eta_{10} \leq 18 \quad (12)$$

Thus, at present, there is no conflict with the CMB inferred value of Y_p .

7. Discussion

One of the key results of the preceding exercise is that despite having apparently high quality data, the final ${}^4\text{He}$ abundance for any given HII region will depend critically on assumptions

concerning the appropriate electron temperature, the presence of underlying absorption, and the treatment of the optical depth effects. Many of the systems analyzed here show significant evidence for underlying absorption which leads to an increase in the derived ^4He abundance. Additionally, many of the systems show significant evidence for non-zero values of $\tau(3889)$ which relies on an untested formula for correction.

Furthermore, as one can see from the results for individual HII regions shown in the tables, the spread in the derived ^4He abundances can be far greater than the derived error for a given solution. This is a clear sign that systematic uncertainties are dominating the error budget. While some of the systematics such as optical depth and underlying absorption move the ^4He abundance in opposite directions, it makes no sense to suppose that these systematic uncertainties cancel each other out and therefore can be ignored as argued in IT04. Nor does it make sense to continuously average literature data to beat down the statistical errors, once again in complete neglect of the systematic uncertainties as attempted in Dmitriev, Flambaum & Webb (2004). In this context, we stress that there is no evidence for a discrepancy between BBN predictions of ^4He using the WMAP baryon density and observational determinations of the ^4He abundance as frequently reported in the literature.

Inherent degeneracies between the parameters allow for very different solutions with equally acceptable χ^2 . This was the main point of our previous work (OS). Perhaps most troubling is the degeneracy in the parameter space identified here between temperature and density. As we noted throughout our analysis, IT98 have fixed the temperature to the OIII temperature which is systematically high (Peimbert, Peimbert, & Luridiana 2002). However, as one can see from eqs. (A2), changes in temperature can be compensated by changes in the density allowing for the possibility of very different results due to various corrections. This may explain the puzzling result that the dispersion in the IT98 helium abundances is actually smaller than their formal errors. By assuming that the OIII temperatures are appropriate to the entire He^+ emission zone, the densities have been biased to unrealistically low values resulting in higher values of the helium abundance. On the other hand, by assuming that underlying He absorption is negligible, the derived helium abundances have been biased to lower values. The narrow range of derived helium abundances may be a result of these biases in the analysis.

There are other potentially important sources for systematic uncertainty such as temperature fluctuations (Steigman, Viegas, & Gruenwald 1997; Sauer & Jedamzik 2002), ionization corrections (Ballantyne, Ferland, & Martin 2000; Viegas, Gruenwald, & Steigman 2000; Gruenwald, Steigman

& Viegas 2002; Sauer & Jedamzik 2002), and the collisional excitation of hydrogen emission lines (Skillman & Kennicutt 1993; Stasińska & Izotov 2001, LPPC). However, it is our impression that these are small compared to the uncertainties that we have focused on here.

From our analyses, it appears that the high EW regions may be more prone to high values of $\tau(3889)$, which makes them less suitable candidates. This could be a real problem for identifying new candidates for high precision helium abundances. If derived helium abundances depend on our simple model for helium optical depth effects, we have a systematic uncertainty which, at present, is not testable. At this point, the prudent thing to do is to exclude all targets with relatively high values of $\tau(3889)$ from any analysis sample (as opposed to trying to correct for such effects).

We suggest that the following efforts will result in future progress on obtaining a more accurate value for the primordial helium abundance. On the observation side:

(1) Significantly higher quality spectra are needed for almost all of the regions studied to date. Concentrating on those objects which appear to have higher $EW(H\beta)$ and low $\tau(3889)$, in addition to low O/H abundance, will be important.

(2) It is still important to search for new targets. Obviously the targets which satisfy the above criteria are rare (Terlevich, Skillman, & Terlevich 1996).

(3) Observations along multiple lines of sight to individual targets will allow testing of our analysis techniques as the physical conditions are changing while (hopefully) the helium abundances are not (e.g., Skillman et al. 1994).

(4) Observations are needed at higher spectral resolution and over a larger wavelength range. The higher resolution (better than 1 \AA) will allow the profiles of the underlying HeI absorption to be observed, and thus allow for better corrections. The larger wavelength range will allow measurements of additional physical parameters (i.e., the temperature in the lower ionization zone from [O II] lines) which will place stronger constraints on the derived physical parameters. Long-slit double spectrographs provide the best tool for this work.

On the theoretical side, work remains in order to better characterize the uncertainties in the current atomic data and the prescriptions by which the observations are converted into abundances (e.g., Porter, Bauman, & Ferland 2003).

In sum, echoing our introduction, pinning down the primordial helium abundance to a higher accuracy remains a worthwhile goal. To significantly decrease the uncertainty in the primordial

helium abundance will require spectra of metal poor HII regions of a quality exceeding most of those present in the literature today and analyses that take into account the several sources of systematic errors which have been identified so far.

We would like to thank R. Benjamin, D. Garnett, R. Kennicutt, D. Kunth, H. Lee, V. Luridiana, B. Pagel, A. Peimbert, M. Peimbert, G. Shields, J. Shields, G. Steigman, S. Viegas, E. Terlevich, and R. Terlevich, for informative and valuable discussions. The work of KAO is supported in part by DOE grant DE-FG02-94ER-40823. EDS is grateful for partial support from a NASA LTSARP grant No. NAG5-9221 and the University of Minnesota. EDS is also grateful to the Institute of Astronomy at the University of Cambridge where much of this work was done while on sabbatical leave from the University of Minnesota.

A. Helium Line Ratios

We again start with a set of observed quantities: line intensities $I(\lambda)$ which include the red-dering correction previously determined in OS and its associated uncertainty and the equivalent width $W(\lambda)$. The Helium line intensities are scaled to $H\beta$ and the singly ionized helium abundance is given by

$$y^+(\lambda) = \frac{I(\lambda)}{I(H\beta)} \frac{F_\lambda(n_e, T)}{f_\lambda(n_e, T, \tau)} \left(\frac{W(\lambda) + a_{HeI}}{W(\lambda)} \right) \quad (\text{A1})$$

where $F_\lambda(n_e, T)$ is the theoretical emissivity scaled to $H\beta$ and the optical depth function f_λ contains the collisional correction. The expression (A1), also contains a correction factor for underlying stellar absorption, parameterized now by a_{HeI} . Thus y^+ implicitly depends on four unknowns, the electron density, n , a_{HeI} , τ , and T .

To be definite, we list here the necessary components in expression (A1). The theoretical emissivities scaled to $H\beta$ are taken from Benjamin, Skillman, & Smits (1999):

$$\begin{aligned} F_{3889} &= 0.904T^{-0.173-0.00054n_e} \\ F_{4026} &= 4.297T^{0.090-0.0000063n_e} \\ F_{4471} &= 2.010T^{0.127-0.00041n_e} \\ F_{5876} &= 0.735T^{0.230-0.00063n_e} \\ F_{6678} &= 2.580T^{0.249-0.00020n_e} \\ F_{7065} &= 12.45T^{-0.917}/(3.4940 - (0.793 - .0015n_e + 0.000000696n_e^2)T) \end{aligned} \quad (\text{A2})$$

Our expressions for the optical depth function which includes the collisional correction is also taken from Benjamin, Skillman, & Smits (1999). We list them here for completeness. They are:

$$\begin{aligned}
 f(3889) &= 1 + (\tau/2) [-0.106 + (5.14 \times 10^{-5} - 4.20 \times 10^{-7}n_e + 1.97 \times 10^{-10}n_e^2)T] \\
 f(4026) &= 1 + (\tau/2) [0.00143 + (4.05 \times 10^{-4} + 3.63 \times 10^{-8}n_e)T] \\
 f(4471) &= 1 + (\tau/2) [0.00274 + (8.81 \times 10^{-4} - 1.21 \times 10^{-6}n_e)T] \\
 f(5876) &= 1 + (\tau/2) [0.00470 + (2.23 \times 10^{-3} - 2.51 \times 10^{-6}n_e)T] \\
 f(6678) &= 1 \\
 f(7065) &= 1 + (\tau/2) [0.359 + (-3.46 \times 10^{-2} - 1.84 \times 10^{-4}n_e + 3.039 \times 10^{-7}n_e^2)T] \quad (\text{A3})
 \end{aligned}$$

Finally we note that we discovered two sign errors in OS concerning the theoretical Balmer line ratios. In Eq. A.3 of that paper, the last two expressions each contain an error. The correct expressions should be: $X_T(4340) = -0.01655(\log T_4)^2 + 0.02824 \log T_4 + 0.468$ and $X_T(4101) = -0.01655(\log T_4)^2 + 0.02159 \log T_4 + 0.259$.

REFERENCES

- Abroe, M.E., *et al.* 2002, MNRAS, 334, 11
- Asplund, M., Grevesse, N., Sauval, A. J., Allende Prieto, C., & Kiselman, D. 2004, A&A, 417, 751
- Ballantyne, D. R., Ferland, G. J., & Martin, P. G. 2000, ApJ, 536, 773
- Benjamin, R. A., Skillman, E. D., & Smits, D. P., 1999, ApJ, 514, 307
- Benjamin, R. A., Skillman, E. D., & Smits, D. P. 2002, ApJ, 569, 288
- Bennett, C.L., *et al.* 2003, ApJS, 148, 1
- Benoit, A. *et al.* 2002, A&A, 399, L25
- Bonifacio, P., *et al.* 2002, AA, 390, 91
- Bradamante, F., Matteucci, F., & D’Ercole, A. 1998, A&A, 337, 338
- Burles, S., Nollett, K.M., & Turner, M.S., 2001, ApJ, 552, L1
- Burles, S. & Tytler, D. 1998a, ApJ, 499, 699

- Burles, S. & Tytler, D. 1998b, *ApJ*, 507, 732
- Cardelli, J. A., Clayton, G. C., & Mathis, J. S. 1989, *ApJ*, 345, 245
- Carigi, L., Colin, P., Peimbert, M., & Sarmiento, A. 1995, *ApJ*, 445, 98
- Coc, A., Vangioni-Flam, E., Descouvemont, P., Adahchour, A., & Angulo, C. 2004, *ApJ*, 600, 544
- Cyburt, R.H., Fields, B.D., & Olive, K.A. 2001, *New Astronomy*, 6, 215
- Cyburt, R.H., Fields, B.D., & Olive, K.A. 2002, *Ast. Part. Phys.*, 17, 87
- Cyburt, R.H., Fields, B.D., & Olive, K.A. 2003, *Phys. Lett.*, B567, 227
- Cyburt, R.H., Fields, B.D., & Olive, K.A. 2004, *astro-ph/0312629*
- Dinerstein, H. L. & Shields, G. A. 1986, *ApJ*, 311, 45
- Dmitriev, V.F., Flambaum, V.V., & Webb, J.K. 2004, *Phys. Rev.* D69, 063506
- Esposito, S., Mangano, G., Miele, G., & Pisanti, O. 2000, *Nucl Phys*, B568, 421
- Fields, B. D., Kainulainen, K., Olive, K. A., & Thomas, D. 1996, *New Astron.*, 1, 77
- Fields, B. D. & Olive, K. A. 1996, *Phys Lett*, B368, 103
- Fields, B.D. & Olive, K.A. 1998, *ApJ*, 506, 177
- Fields, B.D., Olive, K. A., Silk, J., Cassé, M., Vangioni-Flam, E. 2001, *ApJ*, 563, 653
- Fields, B.D. & Sarkar, S. 2002, in K. Hagiwara et al., *Phys. Rev.* D66 010001
- Filippenko, A. V. 1982, *PASP*, 94, 715
- Fiorentini, G., Lisi, E., Sarkar, S., & Villante, F.L. 1998, *Phys Rev*, D58, 063506
- Garnett, D. R. 1992, *AJ*, 103, 1330
- Goldstein, J. H., *et al.* 2003, *ApJ*, 599, 773
- Gruenwald, R., Steigman, G., & Viegas, S. M. 2002, *ApJ*, 567, 931
- Hata, N., Scherrer, R.J., Steigman, G., Thomas, D., & Walker, T.P. 1996, *ApJ*, 458, 637
- Hummer, D. G. & Storey, P. J. 1987, *MNRAS*, 224, 801

- Izotov, Y. I., & Thuan, T. X. 1998, *ApJ*, 500, 188 (IT98)
- Izotov, Y. I., & Thuan, T. X. 2004, *ApJ*, 602, 200
- Izotov, Y. I., Thuan, T. X., & Lipovetsky, V. A. 1994, *ApJ*, 435, 647 (ITL94)
- Izotov, Y. I., Thuan, T. X., & Lipovetsky, V. A. 1997, *ApJS*, 108, 1 (ITL97)
- Kingdon, J., & Ferland, G. 1995, *ApJ*, 442, 714
- Kirkman, D., Tytler, D., Suzuki, N., O’Meara, J., & Lubin, D. 2003, *ApJS*, 149, 1
- Luridiana, V., Peimbert, A., Peimbert, M., & Cerviño, M. 2003, *ApJ*, 592, 846
- Miller, J. S. & Mathews, W. G. 1972, *ApJ*, 172, 593
- Netterfield, C.B. *et al.* , 2002, *ApJ*, 571, 604
- Olive, K.A. & Skillman, E. 2001, *New Astronomy*, 6, 119
- Olive, K.A., Steigman, G. & Walker, T.P. 1991, *ApJ*, 380, L1
- Olive, K. A., Steigman, G. & Walker, T.P. 2000, *Phys Rep*, 333, 389
- O’Meara, J.M., *et al.* 2001, *ApJ*, 522, 718
- Pagel, B. E. J., Simonson, E. A., Terlevich, R. J., & Edmunds, M. G. 1992, *MNRAS*, 255, 325 (PSTE)
- Peimbert, A., Peimbert, M., & Luridiana, V. 2002, *ApJ*, 565, 668
- Peimbert, M., Peimbert, A., & Ruiz, M. T. 2000, *ApJ*, 541, 688
- Percival, W.J., *et al.* 2002, *MNRAS*, 337, 1068
- Perlmutter, S., *et al.* 1999, *ApJ*, 517, 565
- Pettini, M., & Bowen, D.V. 2001, *ApJ*, 560, 41
- Pilyugin, L.S. 1993, *A&A*, 277, 42
- Porter, R. L., Bauman, R. P., & Ferland, G. J. 2003, *Revista Mexicana de Astronomia y Astrofisica Conference Series*, 18, 90
- Pinsonneault, M. H., Walker, T. P., Steigman, G., & Narayanan, V. K. 1999, *ApJ*, 527, 180

- Pinsonneault, M. H., Steigman, G., Walker, T. P., & Narayanan, V. K. 2002, *ApJ*, 574, 398
- Pryke, C., Halverson, N., Leitch, E., Kovac, J., Carlstrom, J., Holzappel, W. & Dragovan, M. 2002, *ApJ*, 568, 46
- Reeves, H., Audouze, J., Fowler, W., & Schramm, D.N. 1976 *ApJ*, 179, 909
- Riess, A.G., *et al.* 1998, *AJ*, 116, 1009
- Robbins, R.R. 1968, *ApJ*, 151, 511
- Rubiño-Martin, J.A. *et al.* 2003, *MNRAS*, 341, 1084
- Ryan, S.G., Beers, T.C., Olive, K.A., Fields, B.D., & Norris, J.E. 2000, *ApJ*, 530, L57
- Ryan, S.G., Norris, J.E., & Beers, T.C. 1999, *ApJ*, 523, 654
- Sarkar, S. 1996, *Rep. Prog. Phys.*, 59, 1493
- Sauer, D. & Jedamzik, K. 2002, *AA*, 381, 361
- Sawey, P. M. J., & Berrington, K. A. 1993, *Atomic Data Nucl. Data Tables*, 55, 81
- Schlegel, D. J., Finkbeiner, D. P., & Davis, M. 1998, *ApJ*, 500, 525
- Sievers, J.L. *et al.* , 2003, *ApJ*, 591, 599
- Skillman, E. D. & Kennicutt, R. C. 1993, *ApJ*, 411, 655
- Skillman, E. D., Terlevich, R. J., Kennicutt, R. C., Garnett, D. R., & Terlevich, E. 1994, *ApJ*, 431, 172
- Skillman, E. D., Terlevich, E., & Terlevich, R. 1998, *Space Science Reviews*, 84, 105
- Smits, D.P. 1996, *MNRAS*, 251, 316
- Spergel, D.N., *et al.*, 2003, *ApJS*, 148, 175
- Stasińska, G. & Izotov, Y. 2001, *A&A*, 378, 817
- Steigman, G., Viegas, S. M. & Gruenwald, R. 1997, *ApJ*, 490, 187
- Tegmark, M., *et al.* 2004, *Phys. Rev. D*69, 103501

Terlevich, E., Skillman, E. D., & Terlevich, R. 1996, *The Interplay Between Massive Star Formation, the ISM and Galaxy Evolution*, 395

Tonry, J.L., *et al.* 2003, *ApJ*, 594, 1

Vauclair, S. & Charbonnel, C. 1998, *ApJ*, 502, 372

Viegas, S. M., Gruenwald, R. & Steigman, G. 2000, *ApJ*, 531, 813

Walker, T.P., Steigman, G., Schramm, D.N., Olive, K.A., & Kang, K. 1991, *ApJ*, 376, 51

Whitford, A. E. 1958, *AJ*, 63, 201

Table 1. He Emission Lines and EW for NGC 346 from PPR00

He I line	$I(\lambda)/I(H\beta)$	EW (\AA)
From PPR00		
$\lambda 5876$	0.1064 ± 0.0012	46 ± 4.6
$\lambda 4471$	0.0384 ± 0.0006	8.5 ± 0.85
$\lambda 6678$	0.0296 ± 0.0003	14.7 ± 1.47
$\lambda 7065$	0.0211 ± 0.0002	11.1 ± 1.11
$\lambda 3889$	0.0940 ± 0.0017	16.1 ± 1.61
$\lambda 4026$	0.0185 ± 0.0006	3.16 ± 0.32
PPR00 (re-analyzed)		
$\lambda 5876$	0.1053 ± 0.0013	46 ± 4.6
$\lambda 4471$	0.0388 ± 0.0005	8.5 ± 0.85
$\lambda 6678$	0.0296 ± 0.0002	14.7 ± 1.47
$\lambda 7065$	0.0210 ± 0.0002	11.2 ± 1.12
$\lambda 3889$	0.0987 ± 0.0022	16.5 ± 1.65
$\lambda 4026$	0.0189 ± 0.0007	3.10 ± 0.31

Table 2. Analysis of NGC 346 from PPR00

Analysis	He ⁺ /H ⁺	T _e < (HeII) >	N _e	He I ABS EW (Å)	τ(3889)	χ ²
PPR00	0.0793 ± 0.0006 (solved)	11,920 ± 370 (solved)	146 ± 50 (solved +)	0 (fixed)	0 (fixed)	...
D	0.0795 ± 0.0005	11,920 ± 370	164 ⁺⁵⁶ ₋₄₇	0	0.00 ^{+0.09} _{-0.00}	3.1
D (re-an)	0.0797 ± 0.0007 (solved)	11,920 ± 370 (fixed)	149 ⁺⁵¹ ₋₄₆ (solved +)	0 (fixed)	0.00 ^{+0.06} _{-0.00} (solved +)	10.0
D	0.0797 ± 0.0006	11,920 ± 370	163 ⁺⁵⁴ ₋₄₉	0.03 ^{+0.12} _{-0.03}	0.00 ^{+0.09} _{-0.00}	3.0
MC	0.0801 ± 0.0011	11,920 ± 370	159 ± 69	0.07 ^{+0.11} _{-0.07}	0.03 ^{+0.13} _{-0.03}	...
D (re-an)	0.0797 ± 0.0007	11,920 ± 370	148 ⁺⁵³ ₋₄₆	0.00 ^{+0.07} _{-0.00}	0.00 ^{+0.06} _{-0.00}	10.0
MC (re-an)	0.0800 ± 0.0009 (solved)	11,920 ± 370 (fixed)	152 ± 63 (solved +)	0.03 ^{+0.09} _{-0.03} (solved +)	0.00 ^{+0.01} _{-0.00} (solved +)	...
D	0.0810 ± 0.0005	12,510 ± 190	89 ⁺²¹ ₋₁₉	0.08 ^{+0.12} _{-0.08}	0.00 ^{+0.07} _{-0.00}	2.4
MC	0.0816 ± 0.0014	12,650 ± 580	67 ⁺⁶⁹ ₋₆₇	0.12 ± 0.11	0.06 ^{+0.14} _{-0.06}	...
D (re-an)	0.0827 ± 0.0005	13,460 ± 230	0.1 ⁺¹² _{-0.1}	0.07 ^{+0.12} _{-0.07}	0.00 ^{+0.04} _{-0.00}	3.7
MC (re-an)	0.0828 ± 0.0008 (solved)	13,420 ± 280 (solved)	2 ⁺¹⁹ ₋₂ (solved +)	0.09 ± 0.09 (solved +)	0.01 ^{+0.04} _{-0.01} (solved +)	...
D	0.0810 ± 0.0005	12,510 ± 190	89 ⁺²¹ ₋₂₀	0.08 ^{+0.12} _{-0.11}	0.00 ^{+0.07} _{-0.00}	2.4
MC	0.0820 ± 0.0014	12,810 ± 540	36 ⁺⁹⁴ ₋₃₆	0.13 ± 0.13	0.13 ± 0.13	...
D (re-an)	0.0827 ± 0.0005	13,460 ± 230	0.3 ⁺¹² _{-0.2}	0.07 ± 0.12	0.00 ^{+0.04} _{-0.00}	3.7
MC (re-an)	0.0827 ± 0.0009 (solved)	13,430 ± 260 (solved)	1 ⁺¹¹ ₋₁ (solved +)	0.07 ^{+0.18} _{-0.07} (solved free)	0.01 ^{+0.06} _{-0.01} (solved +)	...
D	0.0777 ± 0.0005	11,530 ± 150	427 ⁺⁴⁷ ₋₄₂	-0.05 ± 0.11	-0.47 ± 0.07	1.9
MC	0.0813 ± 0.0084	13,000 ± 3,580	376 ± 415	0.10 ± 0.36	0.07 ± 1.14	...
D (re-an)	0.0829 ± 0.0005	13,820 ± 240	22 ± 16	0.06 ± 0.12	-0.24 ± 0.07	2.3
MC (re-an)	0.0836 ± 0.0051 (solved)	14,080 ± 1,770 (solved)	72 ± 223 (solved free)	0.09 ± 0.24 (solved free)	-0.16 ± 0.56 (solved free)	...

Table 3a. He Emission Lines and EW for IT98 “High Quality” Data Sample

He I line	SBS 0335 -025		NGC 2363A		SBS 0940+544		MRK 193	
	I(λ)/I(H β)	EW (\AA)	I(λ)/I(H β)	EW (\AA)	I(λ)/I(H β)	EW (\AA)	I(λ)/I(H β)	EW (\AA)
	from IT98							
λ 5876	0.098 ± 0.002	35.3 ± 3.5	0.106 ± 0.001	63.0 ± 6.3	0.099 ± 0.003	36.7 ± 3.67	0.111 ± 0.002	38.1 ± 3.81
λ 4471	0.037 ± 0.002	6.1 ± 0.6	0.039 ± 0.001	10.9 ± 1.1	0.037 ± 0.002	6.6 ± 0.66	0.039 ± 0.002	6.7 ± 0.67
λ 6678	0.026 ± 0.001	12.5 ± 1.3	0.029 ± 0.001	24.0 ± 2.4	0.026 ± 0.001	12.8 ± 1.28	0.028 ± 0.001	14.5 ± 1.45
λ 7065	0.039 ± 0.001	22.9 ± 2.3	0.029 ± 0.001	29.7 ± 3.0	0.026 ± 0.002	12.3 ± 1.23	0.032 ± 0.002	19.1 ± 1.91
λ 3889	0.064 ± 0.004	7.5 ± 0.8	0.088 ± 0.001	16.8 ± 1.7	0.109 ± 0.007	13.1 ± 1.31	0.100 ± 0.005	9.1 ± 0.91
λ 4026	0.016 ± 0.002	2.0 ± 0.2	0.016 ± 0.001	3.3 ± 0.3	0.021 ± 0.002	2.7 ± 0.27	0.018 ± 0.002	2.0 ± 0.20
	(re-analyzed)							
λ 5876	0.0977 ± 0.0020	35.3 ± 3.5	0.1056 ± 0.0010	63.0 ± 6.3	0.0997 ± 0.0031	36.7 ± 3.67	0.1122 ± 0.0028	38.1 ± 3.81
λ 4471	0.0370 ± 0.0021	6.1 ± 0.6	0.0391 ± 0.0010	10.9 ± 1.1	0.0375 ± 0.0020	6.6 ± 0.72	0.0399 ± 0.0022	6.7 ± 0.73
λ 6678	0.0264 ± 0.0010	12.5 ± 1.3	0.0284 ± 0.0009	24.0 ± 2.4	0.0270 ± 0.0020	12.8 ± 1.88	0.0286 ± 0.0017	14.5 ± 1.71
λ 7065	0.0395 ± 0.0010	22.9 ± 2.3	0.0289 ± 0.0009	29.7 ± 3.0	0.0259 ± 0.0020	12.3 ± 1.88	0.0324 ± 0.0017	19.1 ± 1.97
λ 3889	0.0696 ± 0.0037	7.9 ± 0.8	0.0884 ± 0.0011	16.9 ± 1.7	0.1046 ± 0.0070	12.8 ± 1.70	0.0877 ± 0.0055	8.5 ± 1.05
λ 4026	0.0160 ± 0.0021	2.0 ± 0.5	0.0160 ± 0.0011	3.3 ± 0.4	0.0206 ± 0.0021	2.7 ± 0.54	0.0188 ± 0.0012	2.0 ± 0.25

Table 3b. He Emission Lines and EW for IT98 “High Quality” Data Sample

He I line	SBS 1159+545		Haro 29		SBS 1420+544	
	I(λ)/I(H β)	EW (\AA)	I(λ)/I(H β)	EW (\AA)	I(λ)/I(H β)	EW (\AA)
from IT98						
λ 5876	0.101 ± 0.002	44.3 ± 4.43	0.102 ± 0.001	40.8 ± 4.08	0.101 ± 0.001	35.5 ± 3.55
λ 4471	0.039 ± 0.001	7.2 ± 0.72	0.036 ± 0.001	7.48 ± 0.75	0.037 ± 0.001	6.9 ± 0.69
λ 6678	0.026 ± 0.001	14.3 ± 1.43	0.029 ± 0.001	14.2 ± 1.42	0.028 ± 0.001	12.8 ± 1.28
λ 7065	0.027 ± 0.001	16.6 ± 1.66	0.024 ± 0.001	14.3 ± 1.43	0.037 ± 0.001	20.4 ± 2.04
λ 3889	0.104 ± 0.005	12.5 ± 1.25	0.097 ± 0.001	12.4 ± 1.24	0.085 ± 0.004	11.4 ± 1.14
λ 4026	0.019 ± 0.001	2.60 ± 0.26	0.016 ± 0.001	2.42 ± 0.24	0.018 ± 0.001	2.60 ± 0.26
(re-analyzed)						
λ 5876	0.1018 ± 0.0021	44.3 ± 4.43	0.1017 ± 0.0010	40.8 ± 4.08	0.1006 ± 0.0019	35.5 ± 3.55
λ 4471	0.0386 ± 0.0010	7.2 ± 0.72	0.0366 ± 0.0010	7.5 ± 0.75	0.0376 ± 0.0011	6.9 ± 0.69
λ 6678	0.0267 ± 0.0010	14.3 ± 1.43	0.0286 ± 0.0010	14.2 ± 1.42	0.0283 ± 0.0009	12.8 ± 1.28
λ 7065	0.0274 ± 0.0010	16.6 ± 1.66	0.0247 ± 0.0010	14.3 ± 1.43	0.0373 ± 0.0010	20.4 ± 2.04
λ 3889	0.1033 ± 0.0047	12.3 ± 1.23	0.0969 ± 0.0011	12.3 ± 1.24	0.0893 ± 0.0037	11.4 ± 1.14
λ 4026	0.0197 ± 0.0011	2.60 ± 0.28	0.0158 ± 0.0010	2.42 ± 0.30	0.0187 ± 0.0011	2.60 ± 0.31

Table 4. Analysis of SBS 0335-052 from IT98

Analysis	He ⁺ /H ⁺	T _e < (HeII) >	N _e	He I ABS EW (Å)	τ(3889)	χ ²
IT98	0.080 ± 0.001 (solved)	20,300 ± 300 (solved)	67 ± 3 (solved +)	0 (fixed)	1.7 ± 0.3 (fixed)	...
D	0.0798 ± 0.0016	20,300 ± 300	0.01 ⁺¹⁹ _{-0.01}	0	5.06 ^{+0.32} _{-0.31}	9.9
D (re-an)	0.0808 ± 0.0011 (solved)	20,530 ± 390 (fixed)	0.01 ⁺²³ ₋₀ (solved +)	0 (fixed)	4.98 ^{+0.31} _{-0.30} (solved +)	4.4
D	0.0825 ± 0.0016	20,300 ± 300	0.02 ⁺¹⁷ _{-0.02}	0.48 ^{+0.33} _{-0.27}	4.86 ^{+0.32} _{-0.31}	6.8
MC	0.0827 ± 0.0022	20,300 ± 300	0.3 ⁺⁸ _{-0.3}	0.52 ± 0.34	4.85 ± 0.33	...
D (re-an)	0.0829 ± 0.0014	20,530 ± 390	0.0 ⁺²¹ ₋₀	0.38 ^{+0.33} _{-0.26}	4.82 ± 0.30	2.3
MC (re-an)	0.0832 ± 0.0022 (solved)	20,530 ± 390 (fixed)	3 ⁺²² ₋₃ (solved +)	0.44 ± 0.34 (solved +)	4.78 ± 0.33 (solved +)	...
D	0.0720 ± 0.0013	13,990 ± 660	283 ⁺⁸⁰ ₋₈₈	0.00 ^{+0.22} _{-0.00}	5.22 ^{+0.35} _{-0.34}	0.3
MC	0.0735 ± 0.0042	14,090 ± 2,210	520 ⁺¹³⁸ ₋₅₂₀	0.11 ^{+0.25} _{-0.11}	5.04 ± 0.83	...
D (re-an)	0.0780 ± 0.0016	16,800 ± 1,120	63 ⁺⁷⁰ ₋₆₃	0.13 ^{+0.26} _{-0.13}	4.96 ± 0.31	0.1
MC (re-an)	0.0763 ± 0.0049 (solved)	15,940 ± 2,710 (solved)	347 ⁺⁹⁴¹ ₋₃₄₇ (solved +)	0.14 ^{+0.27} _{-0.14} (solved +)	4.62 ± 0.86 (solved +)	...
D	0.0914 ± 0.0015	32,910 ± 500	0.02 ⁺⁸ _{-0.02}	0.42 ^{+0.28} _{-0.23}	8.59 ± 0.39	0.3
MC	0.0712 ± 0.0055	13,290 ± 2,220	874 ⁺¹²⁴² ₋₈₇₄	-0.01 ± 0.28	4.89 ± 0.90	...
D (re-an)	0.0780 ± 0.0016	16,800 ± 1,120	63 ⁺⁷⁰ ₋₆₃	0.13 ^{+0.26} _{-0.21}	4.96 ± 0.31	0.1
MC (re-an)	0.0755 ± 0.0065 (solved)	15,390 ± 3,190 (solved)	581 ⁺¹²⁷³ ₋₅₈₁ (solved +)	0.08 ± 0.31 (solved free)	4.50 ± 1.03 (solved +)	...
D	0.0716 ± 0.0013	13,850 ± 650	307 ⁺⁸² ₋₈₆	-0.02 ^{+0.23} _{-0.20}	5.20 ± 0.35	0.3
MC	0.0742 ± 0.0072	14,450 ± 3,170	348 ± 438	0.07 ± 0.31	5.28 ± 1.00	...
D (re-an)	0.0780 ± 0.0016	16,800 ± 1,120	63 ⁺⁷⁰ ₋₆₅	0.13 ^{+0.26} _{-0.22}	4.95 ± 0.31	0.1
MC (re-an)	0.0762 ± 0.0098 (solved)	15,730 ± 4,700 (solved)	771 ± 1,040 (solved free)	0.09 ± 0.38 (solved free)	4.57 ± 1.38 (solved free)	...

Table 5. Analysis of NGC 2363A from IT98

Analysis	He ⁺ /H ⁺	T _e < (HeII) >	N _e	He I ABS EW (Å)	τ(3889)	χ ²
IT98	0.081 ± 0.001 (solved)	15,800 ± 100 (solved)	253 ± 10 (solved +)	0 (fixed)	0.0 (fixed)	...
D	0.0840 ± 0.0010	15,800 ± 100	0.4 ⁺⁴⁰ _{-0.4}	0	2.19 ^{+0.16} _{-0.17}	16.5
D (re-an)	0.0840 ± 0.0010 (solved)	15,870 ± 60 (fixed)	0.1 ⁺⁴² _{-0.1} (solved +)	0 (fixed)	2.06 ^{+0.17} _{-0.17} (solved +)	15.2
D	0.0865 ± 0.0007	15,800 ± 100	0.01 ⁺²² _{-0.01}	0.75 ^{+0.23} _{-0.21}	1.98 ^{+0.17} _{-0.18}	2.5
MC	0.0865 ± 0.0010	15,800 ± 100	2.5 ⁺¹⁸ _{-2.5}	0.77 ± 0.24	1.97 ± 0.19	...
D (re-an)	0.0862 ± 0.0008	15,870 ± 60	0.02 ⁺²⁶ _{-0.02}	0.73 ^{+0.24} _{-0.22}	1.87 ^{+0.17} _{-0.18}	2.7
MC (re-an)	0.0861 ± 0.0011 (solved)	15,870 ± 60 (fixed)	6 ⁺²⁹ ₋₆ (solved +)	0.75 ± 0.25 (solved +)	1.85 ± 0.19 (solved +)	...
D	0.0848 ± 0.0009	14,720 ± 510	28 ⁺⁶⁷ ₋₂₈	0.57 ^{+0.21} _{-0.19}	1.84 ± 0.17	0.4
MC	0.0824 ± 0.0042	14,260 ± 1,030	176 ⁺⁴⁰² ₋₁₇₆	0.46 ± 0.28	1.66 ± 0.38	...
D (re-an)	0.0803 ± 0.0009	14,010 ± 460	205 ⁺⁸⁰ ₋₇₄	0.35 ^{+0.21} _{-0.19}	1.45 ± 0.18	0.8
MC (re-an)	0.0801 ± 0.0046 (solved)	14,040 ± 1,060 (solved)	285 ⁺³⁴³ ₋₂₈₅ (solved +)	0.35 ± 0.28 (solved +)	1.44 ± 0.40 (solved +)	...
D	0.0847 ± 0.0009	14,720 ± 510	28 ⁺⁶⁵ ₋₂₈	0.57 ^{+0.21} _{-0.19}	1.84 ± 0.17	0.4
MC	0.0823 ± 0.0046	14,240 ± 1,080	202 ⁺⁵¹² ₋₂₀₂	0.45 ± 0.31	1.65 ± 0.40	...
D (re-an)	0.0804 ± 0.0009	14,150 ± 460	204 ⁺⁷⁸ ₋₇₃	0.35 ^{+0.21} _{-0.19}	1.45 ± 0.18	0.8
MC (re-an)	0.0797 ± 0.0054 (solved)	13,970 ± 1,160 (solved)	346 ⁺⁵⁰⁴ ₋₃₄₆ (solved +)	0.32±0.34 (solved free)	1.41 ± 0.43 (solved +)	...
D	0.0847 ± 0.0009	14,710 ± 510	29 ⁺⁶⁵ ₋₆₁	0.56 ^{+0.21} _{-0.19}	1.84 ± 0.17	0.4
MC	0.0885 ± 0.0105	16,440 ± 3,690	91 ± 406	0.72 ± 0.52	2.29 ± 1.09	...
D (re-an)	0.0804 ± 0.0009	14,020 ± 460	203 ⁺⁷⁹ ₋₇₃	0.35 ^{+0.21} _{-0.19}	1.45 ± 0.18	0.8
MC (re-an)	0.0819 ± 0.0089 (solved)	14,910 ± 3,300 (solved)	311 ± 448 (solved free)	0.42±0.46 (solved free)	1.67 ± 0.94 (solved free)	...

Table 6. Analysis of SBS 0940+544 from IT98

Analysis	He ⁺ /H ⁺	T _e < (HeII) >	N _e	He I ABS EW (Å)	τ(3889)	χ ²
IT98	0.083 ± 0.002 (solved)	20,200 ± 300 (solved)	10 (solved +)	0 (fixed)	0.0 (fixed)	...
D	0.0818 ± 0.0016	20,200 ± 300	72 ⁺⁷³ ₋₆₃	0	0.0 ^{+0.37} _{-0.00}	4.0
D (re-an)	0.0852 ± 0.0019 (solved)	20,200 ± 400 (fixed)	0.3 ⁺⁶⁸ _{-0.3} (solved +)	0 (fixed)	0.35 ^{+0.51} _{-0.35} (solved +)	1.5
D	0.0817 ± 0.0018	20,200 ± 300	75 ⁺⁶⁹ ₋₆₈	0.00 ^{+0.14} _{-0.00}	0.00 ^{+0.35} _{-0.00}	4.0
MC	0.0824 ± 0.0026	20,200 ± 300	67 ± 63	0.05 ^{+0.22} _{-0.05}	0.12 ^{+0.41} _{-0.12}	...
D (re-an)	0.0852 ± 0.0023	20,200 ± 400	0.1 ⁺⁶⁸ _{-0.1}	0.00 ^{+0.24} _{-0.00}	0.35 ^{+0.51} _{-0.35}	1.5
MC (re-an)	0.0852 ± 0.0031 (solved)	20,200 ± 400 (fixed)	22 ⁺⁶¹ ₋₂₂ (solved +)	0.09 ^{+0.33} _{-0.09} (solved +)	0.31 ^{+0.47} _{-0.31} (solved +)	...
D	0.0843 ± 0.0024	22,920 ± 4,110	42 ⁺⁵² ₋₄₂	0.00 ^{+0.20} _{-0.00}	0.00 ^{+0.49} _{-0.00}	3.5
MC	0.0824 ± 0.0043	20,330 ± 2,510	83 ⁺²³⁰ ₋₈₃	0.05 ^{+0.24} _{-0.05}	0.22 ^{+0.45} _{-0.22}	...
D (re-an)	0.0852 ± 0.0027	20,190 ± 3,770	0.5 ⁺⁶⁵ _{-0.5}	0.00 ^{+0.24} _{-0.00}	0.35 ^{+0.51} _{-0.35}	1.5
MC (re-an)	0.0841 ± 0.0035 (solved)	19,260 ± 2,480 (solved)	35 ⁺¹⁴⁰ ₋₃₅ (solved +)	0.07 ^{+0.27} _{-0.07} (solved +)	0.36 ^{+0.46} _{-0.36} (solved +)	...
D	0.0814 ± 0.0025	21,640 ± 3,880	64 ⁺⁶² ₋₅₆	-0.21 ^{+0.30} _{-0.26}	0.00 ^{+0.37} _{-0.00}	3.1
MC	0.0735 ± 0.0105	18,300 ± 3,510	456 ⁺⁵⁸⁷ ₋₄₅₆	-0.46 ± 0.45	0.12 ^{+0.41} _{-0.12}	...
D (re-an)	0.0799 ± 0.0026	18,330 ± 2,510	93 ⁺¹⁰³ ₋₈₄	-0.25 ^{+0.29} _{-0.26}	0.00 ^{+0.44} _{-0.00}	1.2
MC (re-an)	0.0761 ± 0.0111 (solved)	17,970 ± 3,030 (solved)	354 ⁺⁶⁹⁶ ₋₃₅₄ (solved +)	-0.34 ± 0.48 (solved free)	0.23 ^{+0.48} _{-0.23} (solved +)	...
D	0.0705 ± 0.0021	17,960 ± 1,490	394 ⁺¹⁶⁶ ₋₁₃₂	-0.58 ^{+0.24} _{-0.22}	-1.05 ± 0.49	1.6
MC	0.0711 ± 0.0070	18,490 ± 2,560	434 ± 296	-0.55 ± 0.33	-0.73 ± 0.69	...
D (re-an)	0.0732 ± 0.0025	16,870 ± 1,620	318 ⁺²¹⁸ ₋₁₄₄	-0.45 ^{+0.27} _{-0.25}	-0.62 ^{+0.54} _{-0.51}	0.9
MC (re-an)	0.0740 ± 0.0110 (solved)	17,840 ± 2,990 (solved)	420 ± 454 (solved free)	-0.42 ± 0.45 (solved free)	-0.06 ± 0.89 (solved free)	...

Table 7. Analysis of MRK 193 from IT98

Analysis	He ⁺ /H ⁺	T _e < (HeII) >	N _e	He I ABS EW (Å)	τ(3889)	χ ²
IT98	0.081 ± 0.001 (solved)	16,600 ± 200 (solved)	326 ± 65 (solved +)	0 (fixed)	0.0 (fixed)	...
D	0.0784 ± 0.0011	16,600 ± 200	448 ⁺¹⁵⁴ ₋₁₄₀	0	0.56 ± 0.44	1.6
D (re-an)	0.0866 ± 0.0016 (solved)	16,560 ± 200 (fixed)	54 ⁺⁹⁴ ₋₅₄ (solved +)	0 (fixed)	2.16 ^{+0.44} _{-0.42} (solved +)	5.2
D	0.0804 ± 0.0018	16,600 ± 200	387 ⁺¹⁴⁵ ₋₁₂₇	0.15 ^{+0.27} _{-0.15}	0.62 ^{+0.44} _{-0.45}	1.4
MC	0.0813 ± 0.0049	16,600 ± 200	369 ± 188	0.22 ^{+0.27} _{-0.22}	0.74 ± 0.53	...
D (re-an)	0.0896 ± 0.0019	16,560 ± 200	0.04 ⁺⁶⁶ _{-0.04}	0.20 ^{+0.19} _{-0.16}	2.30 ^{+0.43} _{-0.41}	3.8
MC (re-an)	0.0888 ± 0.0035 (solved)	16,560 ± 200 (fixed)	38 ⁺¹⁴² ₋₃₈ (solved +)	0.20 ± 0.18 (solved +)	2.16 ± 0.51 (solved +)	...
D	0.0759 ± 0.0017	14,890 ± 990	637 ⁺¹⁹⁹ ₋₁₇₉	0.00 ^{+0.20} _{-0.00}	0.61 ^{+0.39} _{-0.38}	0.4
MC	0.0781 ± 0.0054	15,500 ± 1,860	607 ± 372	0.11 ^{+0.30} _{-0.11}	0.72 ± 0.49	...
D (re-an)	0.0795 ± 0.0016	12,600 ± 850	524 ± 164	0.00 ^{+0.10} _{-0.00}	1.81 ^{+0.41} _{-0.42}	1.0
MC (re-an)	0.0802 ± 0.0046 (solved)	12,790 ± 1,760 (solved)	820 ⁺⁸⁶⁰ ₋₈₂₀ (solved +)	0.02 ^{+0.13} _{-0.02} (solved +)	1.89 ± 0.70 (solved +)	...
D	0.0746 ± 0.0017	14,640 ± 970	716 ⁺²¹³ ₋₁₉₀	-0.08 ^{+0.22} _{-0.19}	0.62 ± 0.37	0.4
MC	0.0758 ± 0.0071	15,040 ± 2,010	790 ± 513	-0.02 ± 0.33	0.76 ± 0.45	...
D (re-an)	0.0703 ± 0.0015	11,240 ± 460	2,413 ⁺⁸⁴ ₋₁₀₈	-0.27 ± 0.13	1.55 ± 0.15	0.1
MC (re-an)	0.0717 ± 0.0070 (solved)	11,900 ± 1,300 (solved)	1,925 ± 866 (solved +)	-0.24 ± 0.22 (solved free)	1.86 ± 0.80 (solved +)	...
D	0.0746 ± 0.0017	14,630 ± 970	718 ⁺²¹³ ₋₁₉₁	-0.08 ^{+0.22} _{-0.19}	0.62 ± 0.37	0.4
MC	0.0752 ± 0.0068	14,980 ± 1,870	822 ± 511	-0.04 ± 0.32	0.73 ± 0.46	...
D (re-an)	0.0703 ± 0.0015	11,240 ± 460	2,413 ⁺⁸⁴ ₋₁₀₈	-0.27 ± 0.13	1.55 ± 0.15	0.1
MC (re-an)	0.0719 ± 0.0075 (solved)	11,940 ± 1,440 (solved)	1,916 ± 885 (solved free)	-0.23 ± 0.22 (solved free)	1.89 ± 0.85 (solved free)	...

Table 8. Analysis of SBS 1159+545 from IT98

Analysis	He ⁺ /H ⁺	T _e < (HeII) >	N _e	He I ABS EW (Å)	τ(3889)	χ ²
IT98	0.081 ± 0.002 (solved)	18,400 ± 200 (solved)	110 ± 58 (solved +)	0 (fixed)	0 (fixed)	...
D	0.0811 ± 0.0010	18,400 ± 200	130 ⁺⁵³ ₋₄₇	0	0.00 ^{+0.28} _{-0.00}	3.5
D (re-an)	0.0828 ± 0.0011 (solved)	18,570 ± 210 (fixed)	83 ⁺⁴⁷ ₋₄₄ (solved +)	0 fixed	0.31 ^{+0.29} _{-0.28} (solved +)	3.3
D	0.0811 ± 0.0011	18,400 ± 200	129 ⁺⁵² ₋₄₆	0.00 ^{+0.06} _{-0.00}	0.00 ^{+0.28} _{-0.00}	3.5
MC	0.0820 ± 0.0020	18,400 ± 200	100 ± 62	0.01 ^{+0.07} _{-0.01}	0.22 ^{+0.39} _{-0.22}	...
D (re-an)	0.0828 ± 0.0012	18,570 ± 210	83 ⁺⁴⁵ ₋₄₄	0.00 ^{+0.07} _{-0.00}	0.32 ^{+0.28} _{-0.29}	3.3
MC (re-an)	0.0832 ± 0.0021 (solved)	18,570 ± 210 (fixed)	76 ± 62 (solved +)	0.01 ^{+0.08} _{-0.01} (solved +)	0.39 ± 0.37 (solved +)	...
D	0.0825 ± 0.0013	19,460 ± 1,480	93 ⁺⁴⁴ ₋₃₉	0.00 ^{+0.08} _{-0.00}	0.05 ^{+0.28} _{-0.05}	3.3
MC	0.0830 ± 0.0033	19,420 ± 2,100	89 ⁺¹⁰¹ ₋₈₉	0.02 ^{+0.10} _{-0.02}	0.27 ^{+0.39} _{-0.27}	...
D (re-an)	0.0840 ± 0.0014	19,390 ± 1,670	55 ⁺⁴¹ ₋₃₈	0.00 ^{+0.09} _{-0.00}	0.38 ^{+0.28} _{-0.27}	3.2
MC (re-an)	0.0838 ± 0.0031 (solved)	19,330 ± 2,100 (solved)	75 ⁺¹¹⁶ ₋₇₅ (solved +)	0.01 ^{+0.07} _{-0.01} (solved +)	0.45 ± 0.38 (solved +)	...
D	0.0748 ± 0.0013	16,610 ± 860	297 ⁺⁹³ ₋₇₇	-0.32 ^{+0.14} _{-0.13}	0.00 ^{+0.15} _{-0.00}	1.7
MC	0.0725 ± 0.0111	17,550 ± 2,720	529 ± 484	-0.47 ± 0.46	0.15 ^{+0.43} _{-0.15}	...
D (re-an)	0.0741 ± 0.0013	16,280 ± 800	342 ⁺¹⁰² ₋₈₆	-0.38 ^{+0.14} _{-0.13}	0.00 ^{+0.19} _{-0.00}	1.0
MC (re-an)	0.0742 ± 0.0080 (solved)	16,980 ± 2,330 (solved)	434 ± 378 (solved +)	-0.39 ± 0.27 (solved free)	0.17 ^{+0.43} _{-0.17} (solved +)	...
D	0.0697 ± 0.0013	16,570 ± 780	537 ⁺¹⁴³ ₋₁₂₆	-0.48 ± 0.13	-0.52 ± 0.24	0.01
MC	0.0698 ± 0.0058	16,970 ± 1,650	564 ± 276	-0.48 ± 0.22	-0.38 ± 0.44	...
D (re-an)	0.0716 ± 0.0014	16,280 ± 760	466 ⁺¹³⁸ ₋₁₀₉	-0.46 ^{+0.14} _{-0.13}	-0.31 ± 0.26	0.45
MC (re-an)	0.0720 ± 0.0062 (solved)	16,710 ± 1,840 (solved)	493 ± 287 (solved free)	-0.45 ± 0.22 (solved free)	-0.13 ± 0.47 (solved free)	...

Table 9. Analysis of Haro 29 (SBS 1223+487) from IT98

Analysis	He ⁺ /H ⁺	T _e < (HeII) >	N _e	He I ABS EW (Å)	τ(3889)	χ ²
IT98	0.083 ± 0.001 (solved)	16,180 ± 100 (solved)	11 ± 2 (solved)	0 (fixed)	0 (fixed)	...
D	0.0801 ± 0.0009	16,180 ± 100	92 ⁺⁶³ ₋₅₈	0	0.20 ± 0.18	13.4
D (re-an)	0.0789 ± 0.0007 (solved)	16,150 ± 60 (fixed)	144 ⁺⁷⁰ ₋₆₃ (solved +)	0 fixed	0.16 ^{+0.18} _{-0.16} (solved +)	9.2
D	0.0841 ± 0.0009	16,180 ± 100	26 ⁺⁵⁴ ₋₂₆	0.50 ^{+0.17} _{-0.15}	0.20 ± 0.18	2.4
MC	0.0839 ± 0.0017	16,180 ± 100	38 ⁺⁵⁴ ₋₃₈	0.50 ± 0.17	0.20 ± 0.17	...
D (re-an)	0.0827 ± 0.0009	16,150 ± 60	69 ⁺⁵⁷ ₋₅₄	0.42 ^{+0.16} _{-0.15}	0.20 ± 0.19	1.2
MC (re-an)	0.0827 ± 0.0020 (solved)	16,150 ± 60 (fixed)	71 ± 60 (solved +)	0.42 ± 0.16 (solved +)	0.22 ± 0.19 (solved +)	...
D	0.0853 ± 0.0010	16,560 ± 600	0.02 ⁺⁴⁴ _{-0.02}	0.55 ^{+0.17} _{-0.16}	0.31 ± 0.18	2.3
MC	0.0847 ± 0.0019	16,470 ± 780	19 ⁺⁷⁵ ₋₁₉	0.53 ± 0.20	0.27 ± 0.21	...
D (re-an)	0.0854 ± 0.0010	16,960 ± 640	0.1 ⁺⁴⁴ _{-0.1}	0.53 ^{+0.17} _{-0.16}	0.44 ^{+0.18} _{-0.19}	0.8
MC (re-an)	0.0844 ± 0.0024 (solved)	16,760 ± 880 (solved)	31 ⁺¹⁰¹ ₋₃₁ (solved +)	0.50 ± 0.20 (solved +)	0.37 ± 0.24 (solved +)	...
D	0.0853 ± 0.0010	16,560 ± 600	0.1 ⁺⁴⁴ _{-0.1}	0.55 ^{+0.17} _{-0.16}	0.31 ± 0.18	2.3
MC	0.0848 ± 0.0018	16,510 ± 760	14 ⁺⁷⁰ ₋₁₄	0.54 ± 0.20	0.28 ± 0.21	...
D (re-an)	0.0854 ± 0.0010	16,960 ± 640	0.1 ⁺⁴³ _{-0.1}	0.53 ^{+0.17} _{-0.16}	0.44 ± 0.19	0.8
MC (re-an)	0.0846 ± 0.0022 (solved)	16,810 ± 840 (solved)	25 ⁺⁹⁷ ₋₂₅ (solved +)	0.50 ± 0.19 (solved free)	0.38 ± 0.24 (solved +)	...
D	0.0922 ± 0.0011	18,650 ± 700	-125 ⁺³¹ ₋₂₉	0.81 ^{+0.19} _{-0.18}	0.98 ± 0.18	1.9
MC	0.0905 ± 0.0068	18,430 ± 2,190	-60 ± 151	0.74 ± 0.32	0.88 ± 0.69	...
D (re-an)	0.0909 ± 0.0011	18,620 ± 760	-100 ⁺³³ ₋₃₁	0.73 ^{+0.19} _{-0.17}	0.98 ± 0.18	0.6
MC (re-an)	0.0896 ± 0.0075 (solved)	18,680 ± 2,440 (solved)	-32 ± 175 (solved free)	0.67 ± 0.33 (solved free)	0.96 ± 0.75 (solved free)	...

Table 10. Analysis of SBS 1420+544 from IT98

Analysis	He ⁺ /H ⁺	T _e < (HeII) >	N _e	He I ABS EW (Å)	τ(3889)	χ ²
IT98	0.082 ± 0.002 (solved)	17,600 ± 100 (solved)	26 ± 7 (solved +)	0 (fixed)	1.8 ± 0.3 (solved)	...
D	0.0797 ± 0.0007	17,600 ± 100	128 ⁺⁵⁶ ₋₅₂	0	3.17 ± 0.28	2.3
D (re-an)	0.0808 ± 0.0009 (solved)	17,850 ± 120 (fixed)	119 ⁺⁵² ₋₄₈ (solved +)	0 fixed	3.04 ± 0.27 (solved +)	3.6
D	0.0807 ± 0.0010	17,600 ± 100	98 ⁺⁵⁶ ₋₅₂	0.07 ^{+0.15} _{-0.07}	3.28 ± 0.28	2.2
MC	0.0811 ± 0.0025	17,600 ± 100	92 ± 83	0.11 ± 0.12	3.32 ± 0.44	...
D (re-an)	0.0808 ± 0.0011	17,850 ± 120	120 ⁺⁵² ₋₅₀	0.00 ^{+0.12} _{-0.00}	3.04 ± 0.27	3.6
MC (re-an)	0.0815 ± 0.0024 (solved)	17,850 ± 120 (fixed)	110 ± 79 (solved +)	0.04 ^{+0.14} _{-0.04} (solved +)	3.08 ± 0.43 (solved +)	...
D	0.0852 ± 0.0013	19,160 ± 1,710	2 ⁺⁴⁰ ₋₂	0.23 ^{+0.17} _{-0.15}	3.54 ± 0.28	2.0
MC	0.0831 ± 0.0035	18,680 ± 1,700	56 ⁺¹¹⁶ ₋₅₆	0.16 ± 0.17	3.43 ± 0.39	...
D (re-an)	0.0866 ± 0.0015	20,940 ± 2,290	0.3 ⁺³⁰ _{-0.3}	0.13 ^{+0.19} _{-0.13}	3.41 ± 0.27	2.3
MC (re-an)	0.0854 ± 0.0026 (solved)	20,370 ± 1,740 (solved)	27 ⁺⁸³ ₋₂₇ (solved +)	0.12 ^{+0.18} _{-0.12} (solved +)	3.32 ± 0.35 (solved +)	...
D	0.0852 ± 0.0013	19,130 ± 1,710	4 ⁺³⁹ ₋₄	0.22 ^{+0.16} _{-0.15}	3.52 ± 0.28	2.0
MC	0.0804 ± 0.0077	17,280 ± 3,640	419 ^{+1,039} ₋₄₁₉	0.06 ± 0.30	3.11 ± 0.74	...
D (re-an)	0.0866 ± 0.0015	20,950 ± 2,290	0.3 ⁺³⁰ _{-0.3}	0.13 ^{+0.19} _{-0.16}	3.41 ± 0.27	2.3
MC (re-an)	0.0860 ± 0.0030 (solved)	20,600 ± 2,070 (solved)	25 ⁺³⁵⁹ ₋₂₅ (solved +)	0.11 ± 0.20 (solved free)	3.44 ± 0.34 (solved +)	...
D	0.0854 ± 0.0012	19,200 ± 1,720	-1 ⁺¹⁸ ₋₁₈	0.23 ^{+0.16} _{-0.15}	3.55 ± 0.28	1.96
MC (re-an)	0.0802 ± 0.0091	17,340 ± 3,920	459 ± 746	0.06 ± 0.34	3.14 ± 0.92	...
D (re-an)	0.0870 ± 0.0016	21,150 ± 2,240	-6 ⁺²⁹ ₋₂₈	0.14 ^{+0.19} _{-0.16}	3.46 ^{+0.27} _{-0.26}	2.3
MC (re-an)	0.0855 ± 0.0057 (solved)	20,450 ± 2,400 (solved)	72 ± 309 (solved free)	0.10 ± 0.26 (solved free)	3.41 ± 0.58 (solved free)	...

Table 11. Summary of Re-Analysis of IT98 “High Quality” Data Sample

Name	T (K)	n (cm ⁻³)	$\tau(3889)$	He(ABS) (EW)	He ⁺ /H ⁺	He ⁺⁺ /H ⁺	Y	O/H $\times 10^4$
IT98								
SBS 0335-052	20,300 \pm 300	67 \pm 3	1.7 \pm 0.3	0	0.080 \pm 0.001	0.002 \pm 0.001	0.2488 \pm 0.0044	0.19 \pm 0.01
NGC 2363A	15,800 \pm 100	253 \pm 10	0.0	0	0.081 \pm 0.001	0.001 \pm 0.001	0.2456 \pm 0.0008	0.71 \pm 0.01
SBS 0940+544N	20,200 \pm 300	10	0.0	0	0.082 \pm 0.002	0.000	0.2500 \pm 0.0057	0.27 \pm 0.01
MRK 193	16,600 \pm 200	326 \pm 65	0.0	0	0.081 \pm 0.001	0.001 \pm 0.001	0.2478 \pm 0.0037	0.64 \pm 0.01
SBS 1159+545	18,400 \pm 200	110 \pm 58	0.0	0	0.081 \pm 0.002	0.001 \pm 0.001	0.2456 \pm 0.0049	0.31 \pm 0.01
HARO 29	16,180 \pm 100	11 \pm 2	0.0	0	0.083 \pm 0.001	0.001 \pm 0.001	0.2509 \pm 0.0012	0.59 \pm 0.01
SBS 1420+544	17,600 \pm 100	26 \pm 7	1.8 \pm 0.3	0	0.082 \pm 0.001	0.001 \pm 0.001	0.2497 \pm 0.0030	0.56 \pm 0.01
Our Re-analysis								
SBS 0335-052	15,940 \pm 2,710	347 $^{+942}_{-347}$	4.6 \pm 0.9	0.1 $^{+0.2}_{-0.1}$	0.0763 \pm 0.0049	0.0023 \pm 0.0023	0.2391 \pm 0.0116	0.19 \pm 0.01
NGC 2363A	14,040 \pm 1,060	285 $^{+343}_{-285}$	1.4 \pm 0.4	0.35 \pm 0.28	0.0801 \pm 0.0046	0.0008 \pm 0.0008	0.2441 \pm 0.0107	0.69 \pm 0.01
SBS 0940+544N	19,260 \pm 2,480	35 $^{+140}_{-35}$	0.4 \pm 0.4	0.1 $^{+0.3}_{-0.1}$	0.0841 \pm 0.0035	0.000	0.2516 \pm 0.0078	0.26 \pm 0.01
MRK 193	12,790 \pm 1,760	820 $^{+860}_{-820}$	1.9 \pm 0.7	0.0 $^{+0.1}_{-0.0}$	0.0802 \pm 0.0046	0.0011 \pm 0.0011	0.2451 \pm 0.0107	0.61 \pm 0.02
SBS 1159+545	19,330 \pm 2,100	75 $^{+116}_{-75}$	0.5 \pm 0.4	0.0 $^{+0.1}_{-0.0}$	0.0838 \pm 0.0031	0.0010 \pm 0.0010	0.2531 \pm 0.0073	0.30 \pm 0.01
HARO 29	16,680 \pm 890	33 $^{+97}_{-33}$	0.4 \pm 0.2	0.5 \pm 0.2	0.0844 \pm 0.0024	0.0010 \pm 0.0010	0.2543 \pm 0.0058	0.58 \pm 0.01
SBS 1420+544	20,370 \pm 1,740	27 $^{+83}_{-27}$	3.3 \pm 0.4	0.1 $^{+0.2}_{-0.1}$	0.0854 \pm 0.0026	0.0011 \pm 0.0011	0.2568 \pm 0.0062	0.54 \pm 0.01

Table 12. Summary of Re-Analysis of IT04 “High Quality” Data Sample

Name	T (K)	n (cm ⁻³)	$\tau(3889)$	He(ABS) (EW)	He ⁺ /H ⁺	He ⁺⁺ /H ⁺	Y	O/H $\times 10^5$
IT04								
J 0519+0007	20,740 \pm 340	0	0.0783 \pm 0.0015	0.0023 \pm 0.0002	0.2437 \pm 0.0047	2.70 \pm 0.09
HS 2236+1344	21,120 \pm 290	0	0.0789 \pm 0.0013	0.0010 \pm 0.0001	0.2421 \pm 0.0040	2.96 \pm 0.08
HS 0122+0743	17,740 \pm 230	0	0.0826 \pm 0.0013	0.0007 \pm 0.0001	0.2497 \pm 0.0042	3.97 \pm 0.11
HS 0837+4717	19,510 \pm 240	0	0.0763 \pm 0.0011	0.0021 \pm 0.0001	0.2386 \pm 0.0034	3.98 \pm 0.10
CGCG 007-025	16,470 \pm 170	0	0.0786 \pm 0.0009	0.0012 \pm 0.0001	0.2417 \pm 0.0029	5.96 \pm 0.14
HS 0134+3415	16,390 \pm 180	0	0.0812 \pm 0.0013	0.0005 \pm 0.0002	0.2459 \pm 0.0042	7.20 \pm 0.19
HS 1028+3843	15,820 \pm 160	0	0.0800 \pm 0.0011	0.0012 \pm 0.0001	0.2449 \pm 0.0035	7.81 \pm 0.20
Our Re-analysis								
J 0519+0007	22,050 \pm 1,910	335 \pm 189	2.09 \pm 0.86	0.18 \pm 0.27	0.0799 \pm 0.0070	0.0022 \pm 0.0022	0.2471 \pm 0.0166	2.46 \pm 0.10
HS 2236+1344	22,740 \pm 2,230	139 \pm 226	4.52 \pm 0.71	0.38 \pm 0.40	0.0852 \pm 0.0057	0.0009 \pm 0.0009	0.2560 \pm 0.0129	2.76 \pm 0.09
HS 0122+0743	18,860 \pm 2,210	31 \pm 107	0.72 \pm 0.43	1.19 \pm 0.32	0.0887 \pm 0.0041	0.0007 \pm 0.0007	0.2632 \pm 0.0089	3.81 \pm 0.12
HS 0837+4717	21,850 \pm 1,760	303 \pm 112	4.36 \pm 0.61	0.01 \pm 0.03	0.0835 \pm 0.0038	0.0020 \pm 0.0020	0.2547 \pm 0.0095	3.64 \pm 0.13
CGCG 007-025	20,180 \pm 2,210	85 \pm 116	0.87 \pm 0.49	0.43 \pm 0.30	0.0894 \pm 0.0051	0.0012 \pm 0.0012	0.2657 \pm 0.0114	5.69 \pm 0.19
HS 0134+3415	18,160 \pm 2,370	108 \pm 205	1.06 \pm 0.58	0.25 \pm 0.31	0.0840 \pm 0.0051	0.0005 \pm 0.0005	0.2523 \pm 0.0115	6.86 \pm 0.20
HS 1028+3843	17,530 \pm 2,940	461 \pm 448	5.35 \pm 0.88	0.03 \pm 0.14	0.0880 \pm 0.0050	0.0012 \pm 0.0012	0.2626 \pm 0.0113	7.55 \pm 0.23